Fuel 334 (2023) 126643

Contents lists available at ScienceDirect

Fuel

journal homepage: www.elsevier.com/locate/fuel

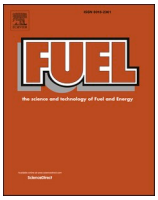

Simulation case studies of aqueous formate solution for geological carbon storage

Oluwafemi Precious Oyenowo, Kai Sheng, Ryosuke Okuno *

Hildebrand Department of Petroleum and Geosystems Engineering, The University of Texas at Austin, Austin, TX 78712, USA

ARTICLE INFO

Keywords:
Geological carbon storage
CO_2
Carbon
Formate
Electrochemical reduction
Enhanced oil recovery

ABSTRACT

Carbon storage in geologic formations has been considered an important technology that reduces the carbon intensity of industrial processes based on fossil fuels. Carbon capture and storage (CCS) conventionally uses carbon dioxide (CO_2) as a carrier. However, various shortcomings of the conventional CCS are related to the physical properties of CO_2, such as low carbon density at low to moderate pressure, low mass density, low viscosity, immiscibility with water, and corrosivity. In particular, CO_2 injection often results in inefficient use of pore space in the formation under geophysical heterogeneities.

This paper presents case studies of using aqueous formate solution as carbon-bearing water for geological carbon storage. Properties of aqueous formate solutions were measured. Experimental results showed that the formate solubility in 102,600-ppm NaCl + $CaCl_2$ brine ranged from 30 wt% to 35 wt% between 25 and 75 °C. Viscosities of 30 wt% formate solutions in the brine were approximately 12 cp at 25 °C, 5 cp at 50 °C, and 3 cp at 75 °C with Newtonian behavior.

Numerical reservoir simulations were performed for an aquifer and an oil reservoir. Simulation results consistently showed that the formate injection case resulted in more stable fronts of oil and water displacement. The more stable fronts yielded the oil recovery and carbon storage that were insensitive to the injectant breakthrough. This is a substantial advantage of using formate as a carbon carrier for controlling the risk of CCS associated with the permeability heterogeneities and their impact on the subsurface flow regime.

The case study of enhanced oil recovery and carbon storage in an oil reservoir showed that the net present value (NPV) of the formate injection case would be equivalent to that of the CO_2 injection case when the cost of CO_2 electrochemical reduction (ECR) into formate was \$269/t-CO_2 for year 20. The breakeven cost of CO_2 ECR for the formate injection case was \$575/t-CO_2 for year 20. Although the estimated CO_2 ECR costs are sensitive to many factors, they are not unrealistically higher than the current costs of CO_2 ECR reported in the literature.

1. Introduction

The Intergovernmental Panel on Climate Change in their sixth assessment report stated that the global warming threshold of 2 °C would be exceeded before the end of the 21st century without large-scale reductions in carbon dioxide (CO_2) emissions [1]. Carbon storage in geologic formations has been identified as an important technology to keep the sustainable growth of countries. Oil reservoirs and deep saline aquifers are the most attractive formations because the large storage capacities are estimated for these formations based on the available data from previous injection projects [2–4].

Current carbon storage processes involve the compression of captured CO_2 into supercritical CO_2, which has a liquid-like density, but a gas-like viscosity. It is necessary to store CO_2 in its supercritical state for more mass of CO_2 to be stored in a given volume. When CO_2 is injected into subsurface formations, some of it dissolves in reservoir brine acidifying the brine, some of it gets trapped in small pores due to capillary pressure between CO_2 and the in-situ fluid, some of it reacts with the ions and minerals in the formation to form minerals, while some of it moves upwards until it reaches a seal because it is less dense than the in-situ fluids. CO_2 is only sparing soluble in brine, and its solubility decreases with salinity and temperature. The capillary trapping and mineralization processes are estimated to take years to thousands of years; hence, it is important to maintain the integrity of the sealing structures and hydraulic paths (faults, impermeable rocks, abandoned wells) in the formation to ensure that the injected CO_2 does not leak into

* Corresponding author.
E-mail address: okuno@austin.utexas.edu (R. Okuno).

https://doi.org/10.1016/j.fuel.2022.126643
Received 15 July 2022; Received in revised form 6 October 2022; Accepted 2 November 2022

overlaying potable water aquifers or into the atmosphere through abandoned wells and unexpected hydraulic paths [3,4,6,10,16,69].

The challenges and risks involved with carbon storage include the following:

a) Costs: One of the challenges to large-scale CO_2 capture and storage is the substantial costs associated with the anthropogenic-CO_2 capture, compression, transportation, and recycling after CO_2 breakthrough at production wells [46,62,65,77,78]. The compression, transportation, and handling of CO_2 can be costly particularly because this corrosive gas has low densities at subcritical conditions, and also because CO_2 storage locations are not correlated to CO_2 emission locations.
b) Inefficient use of storage pore space: CO_2 injection leads to multiphase flow in the subsurface (e.g., gas and water, and gas, oil, and water). Studies in CO_2 EOR have shown that the gas-like viscosity and unfavorable mobility of CO_2 can lead to viscous fingering and significant channeling, leading to inefficient use of pore space in the multiphase displacements of oil and water by CO_2 in heterogeneous media [7,16,37,57,63].
c) Corrosion of pipelines, wells, and cement: When CO_2 dissolves in water, it forms carbonic acid which attacks and corrodes steel surfaces, and also cement in wells. Such corrosion could lead to leakage sites by which CO_2 escapes into the atmosphere [14,17,26,37,64,68,75].
d) Leakage of CO_2 through unexpected hydraulic paths: CO_2 buoyancy-driven flux towards the top of the formation presents the risk of possible leakage through unexpected hydraulic paths (e.g., reactivated faults, fractures, and abandoned wells) to the surface. This risk of leakage can be higher in saline aquifers than in oil and gas reservoirs, because the latter should have accumulated the information of reservoir characterization from years of oil and gas production and exploration. However, the risk of this happening in oil and gas reservoirs is not zero because a possibility of fault reactivation arises by pressure increase during injection, and also geochemical interactions with the cap rock. There is also a possibility of CO_2 escape from abandoned wells with compromised integrity [3,19,30,34,78].

These problems are closely related to the physical properties of CO_2.

This research is concerned with the novel idea of using a formate solution as an aqueous carbon carrier for geological carbon storage. Formate ($HCOO^-$) is the simplest member of the carboxylate group and the conjugate base for formic acid. Formate/formic acid is a high-value product from CO_2 electrochemical reduction (ECR) [38,48]. Currently, formate is produced industrially via the carbonylation of methanol and the hydrolysis of the resulting methyl formate [41]. Because of the need to reduce carbon emissions, the electrochemical conversion of CO_2 into formate and other useful products has been gaining traction. Upscaling of the formate production (from ECR) has been limited by the mass transport of CO_2 in aqueous electrolytes at ambient pressure and temperature [61]. However, recent studies on the CO_2 ECR into formate showed that using gas diffusion electrodes greatly improved the mass transfer process and presented a possibility of industrial scaling of the CO_2 ECR into formate [22,55,61].

The CO_2 ECR into formate is rated a technology readiness level (TRL) of 5, which means the technology has been validated in the laboratory but is still being validated in industrially relevant environments [47]. The field deployment of this technology is not far-off, with various projects such as OCEAN (Oxalic acid from CO_2 using Electrochemistry At demonstratioN scale) already taking the technology to a TRL of 6, only one level lower than field deployment [31]. Some of the technical challenges for the CO_2 ECR technology include the development of an efficient product separation process, electrode degradation/failure due to product accumulation at reaction sites, high power consumption, and optimization of reactor design [8,48,61,66,67].

Baghishov et al. [13] showed that a formate solution can improve oil recovery by altering the wettability of a carbonate rock from oil-wet to water-wet with a slight pH adjustment. Previous studies on formate brine as base fluids for drilling mud have shown that formate salts have favorable health, safety, and environmental (HSE) profiles and have good compatibility with oilfield equipment [28,29,43]. Laboratory tests and field experience in high-pressure high-temperature drilling applications also showed that formate brines have low to minimal corrosion rates, with only one metal failure reported across hundreds of field applications [21,28,44].

This paper presents the use of an aqueous formate solution as a carbon carrier through two case studies: one for carbon storage in an aquifer and the other for enhanced oil recovery (EOR) and carbon storage in an oil reservoir. We also report new experimental data on solubility, density, and viscosity of sodium formate solutions in brines, which set the basis for the numerical flow simulations in this research. Although this paper is centered on the geological carbon storage, use of formate solution can increase the flexibility in the surface operations and facilities in conventional CO_2 geological storage. For example, CO_2 can be converted into formate species near the emission point, transported as formate/formic acid solution, and dehydrogenated for CO_2 geological storage while delivering high-pressure hydrogen gas [60].

2. Measurement of formate solution properties

Since the properties of formate solutions are relatively scarce in the literature [27,29,43,59], we measured new data on solubilities of formate species in brines, and viscosities and densities of formate solutions as part of this research. The results were used to set up numerical flow simulations for the case studies to be presented in Section 3.

2.1. Materials and methods

Sodium formate, sodium chloride, and calcium chloride dihydrate salts (all in a purity >99%) were used in the preparation of brines and formate solutions used in this research. The weighing balance used for mass measurements had an accuracy of ±0.0001 g. All the experiments were done under atmospheric pressure.

2.1.1. Solubility of sodium formate in deionized water (DIW)

The solubility of sodium formate in DIW was determined by preparing aqueous formate solutions of different molarities, allowing them to equilibrate, and observing the maximum molarity at which there were no undissolved salts. Fig. 1 shows prepared sodium formate solutions with different molarities at 25 °C. Formic acid was added to the solutions to adjust the pH to 7. The solubility experiments were done at 25, 50, and 75 °C.

The concentrations of formic acid added to the solutions were calculated using the Henderson-Hasselbalch equation,

$$pH = pKa + log_{10}\frac{[A^-]}{[HA]}$$

where Ka is the acid dissociation constant, pKa is the negative logarithm of Ka ($pKa = -log_{10}Ka$), $[HA]$ is the molar concentration of acid, and $[A^-]$ is the molar concentration of the conjugate base. The acid dissociation constants at 50 and 75 °C were calculated based on a model reported by Kim et al. [49].

2.1.2. Solubility of sodium formate in $NaCl$+$CaCl_2$ brine

To determine the solubility of sodium formate in brine, we dissolved sodium formate in NaCl+$CaCl_2$ brine (97,897 ppm NaCl and 4749 ppm $CaCl_2$). We made several solutions of sodium formate in the brine, each with different weight fractions of sodium formate. The solutions were allowed to equilibrate and the solution with the highest weight fraction

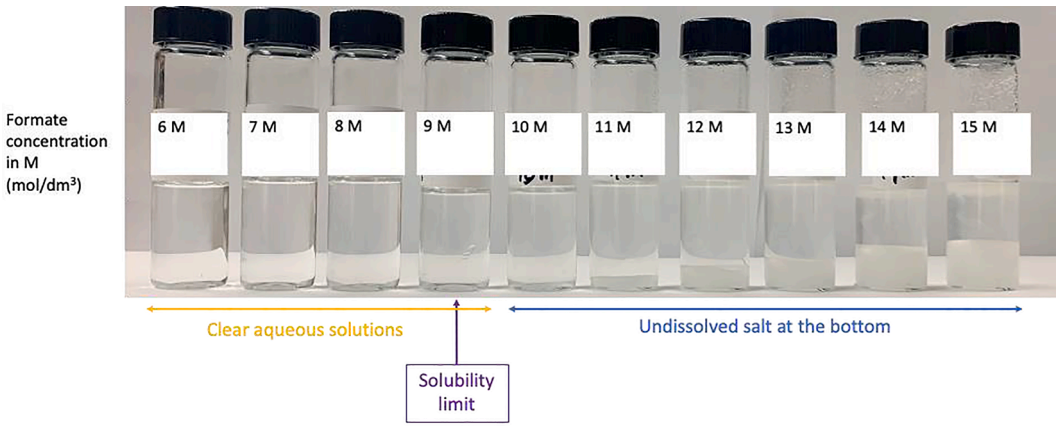

Fig. 1. Sodium formate solutions in DIW at 25 °C. The undissolved salts settled at the bottom. The solution with the highest molar concentration of sodium formate with undissolved salt was chosen as the solubility limit and the weight fraction of formate in the solution was recorded.

of sodium formate added without undissolved salt was recorded, after the initial and fine screening. This experiment was done at 25, 50, and 75 °C. The pH values of the solutions were adjusted by adding formic acid as described previously.

This particular brine containing NaCl and $CaCl_2$ was used since it is common to have divalent cations in formation brine. The addition of $CaCl_2$ was to include the effect of divalent cations without exploring a large number of possible brine compositions for formation brine. A separate research project is necessary to develop a database of formate solution properties in brines.

2.1.3. Viscosity measurements

The viscosities of solutions of different concentrations of sodium formate in the brine (97,897 ppm NaCl and 4749 ppm $CaCl_2$) were measured using a TA Ares LS-1 rheometer coupled with a circulating bath for temperature control. A double wall couette geometry was used for the measurement. The viscosity measurements were performed at 25, 50, and 75 °C. The sodium formate solutions were prepared and allowed to equilibrate in an oven set at the target temperature.

For viscosity measurements at 50 and 75 °C, the temperature of the holding cup was raised to the target temperature using the circulating bath before putting the solution into the rheometer's sample holding cup. This was to avoid precipitation of dissolved salts in samples with a high concentration of formate (e.g., > 30 wt%), which might happen because of a reduced solubility of sodium formate at lower temperature.

2.2. Experimental results

This section reports the formate ion ($HCOO^-$) concentrations in the solutions measured in this research. Note that the formate weight fraction is different from sodium formate (HCOONa) weight fraction in solution. Also, note that each mole of $HCOO^-$ contains one mole of carbon, and the molar mass of $HCOO^-$ is similar to that of CO_2 (45.018 and 44.01 g/mol respectively); therefore, the solubility values of formate are close to the mass fractions of CO_2 held in aqueous form.

Table 1 shows the solubility values of sodium formate in DIW; the solubility of formate in DIW increased with increasing temperature, from 31.5 wt% at 25 °C to 36.77 wt% at 75 °C. The formate solubility measured at 25 °C was close to the result, 32.2 wt%, as reported by Lide [56].

Brines found in geologic formations are often highly saline. Sodium formate was dissolved in brine (salt composition: 97,897 ppm NaCl and 4749 ppm $CaCl_2$) at 25, 50, and 75 °C to determine the solubility at these temperatures and to see if the solution remains single-phase without any precipitation. Table 2 shows the solubility of sodium formate in the brine at 25, 50, and 75 °C. The solubility of formate in the brine ranged from 29.6 wt% at 25 °C to 34.8 wt% at 75 °C.

Newtonian behavior was consistently observed in this research through the viscosity measurements of different solutions of sodium formate in the brine at 25, 50, and 75 °C over a wide range of shear rates as shown in Fig. 2. The viscosity of the formate solutions increased with increasing formate concentration, and a linear trend was observed when viscosity was plotted against the molar concentration of formate on a semi-log scale as shown in Fig. 3 at 25, 50, and 75 °C. The densities and viscosities of sodium formate in the NaCl+$CaCl_2$ brine at 25, 50, and 75 °C are provided in Tables 3, 4, and 5. As a reference, Downs [29] reported the viscosity of near-saturated 45% (% w/w) sodium formate in water to be 9.5 cp at 20 °C.

3. Numerical simulation case studies

Injection of high-pressure CO_2 into hydrocarbon reservoirs and saline aquifers has been studied and implemented for reducing the carbon intensity of industrial processes based on fossil fuels. The central question in this research is whether aqueous formate injection can be a viable option for geological carbon storage in saline aquifers and hydrocarbon reservoirs that improves the various issues associated with CO_2 injection.

The cost of capturing and storing CO_2 is one of the barriers to the global deployment of large-scale carbon capture and storage operations [2]. For the formate injection scenario, the cost of CO_2 ECR into formate will be particularly important. Therefore, the main objective of the

Table 1
Solubilities of sodium formate in DIW.

Temperature (°C)	Aqueous formate solution concentration (M)	Formate concentration (% w/w)	Sodium formate concentration (% w/w)	Density (kg/m³)
25	9	31.50	47.56	1330
50	10	34.38	51.91	1350
75	11	36.77	55.52	1370

Table 2
Solubility of sodium formate in brine at 25, 50, and 75 °C. The brine had a total salinity of 102,646 ppm (97,897 ppm NaCl and 4749 ppm $CaCl_2$).

Temperature (°C)	Formate concentration (% w/w)	Sodium formate concentration (% w/w)	Density (kg/m³)
25.0	29.60	44.72	1367.5
50.0	32.00	48.34	1379.5
75.0	34.78	52.55	1438.8

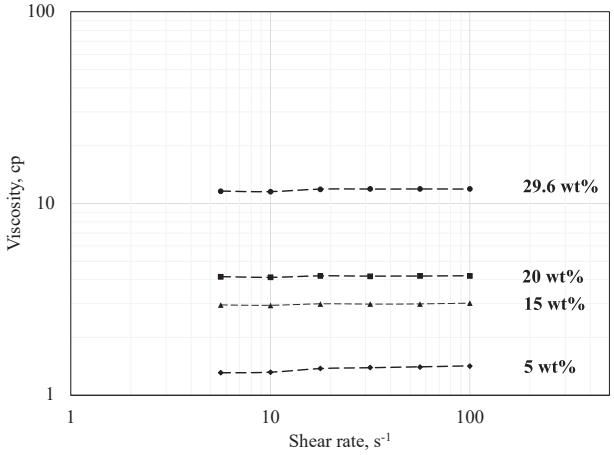

a. Viscosity data for formate solutions in brine at 25°C

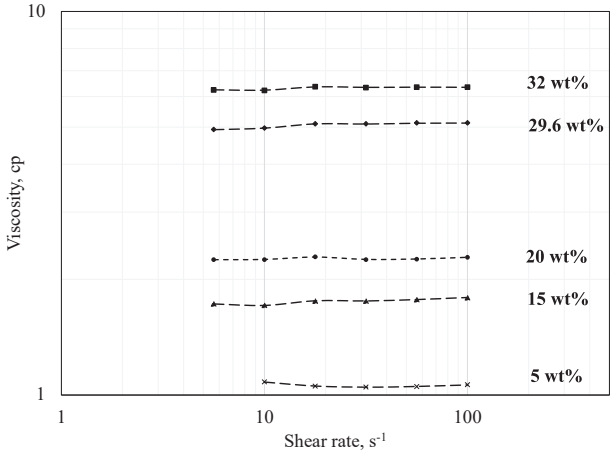

b. Viscosity data for formate solutions in brine at 50°C

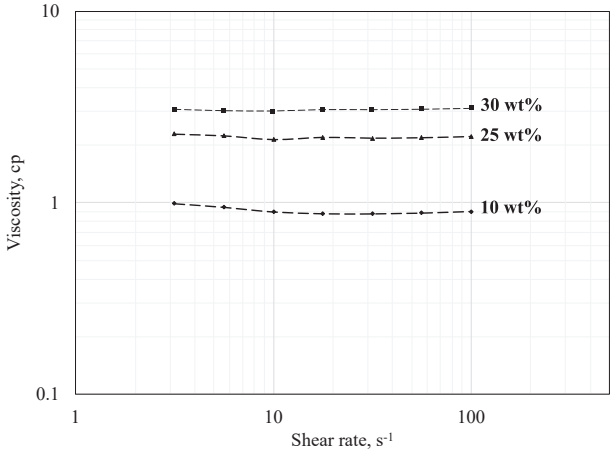

c. Viscosity data for formate solutions in brine at 75°C

Fig. 2. Viscosities of formate solutions in brine at 25, 50 and 75 °C at different shear rates. The measurements showed Newtonian behavior.

simulation case studies is to calculate the cost for the ECR process, below which the formate case resulted in a greater NPV than the CO_2 case. The results will be useful for the research and development of CO_2 ECR systems for large-scale carbon storage applications. As a reference, Somoza-Tornos et al. [73] reported that the market price of formic acid was $500/t in the United States in 2019, and that the reported costs of CO_2 ECR into formic acid ranged widely from $100 to $2630/t.

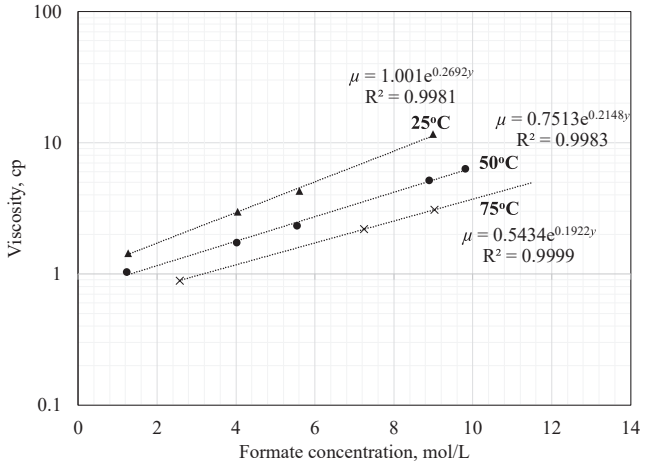

Fig. 3. Viscosities of formate solutions in brine at 25, 50, and 75 °C. The data shows a clear correlation as a logarithmic function of formate molar concentration (y).

Table 3
Densities and viscosities of formate solutions in brine at 25 °C. The brine had a total salinity of 102,646 ppm (97,897 ppm NaCl and 4749 ppm $CaCl_2$).

Formate concentration (% w/w)	Molar concentration (mol/L)	Density @ 25 °C (kg/m^3)	Viscosity @ 25 °C (cp)
5% formate solution	1.26	1136.0	1.44
15% formate solution	4.05	1214.0	2.97
20% formate solution	5.61	1262.5	4.30
29.6% formate solution	9.00	1367.5	11.61

Table 4
Densities and viscosities of formate solutions in brine at 50 °C. The brine had a total salinity of 102,646 ppm (97,897 ppm NaCl and 4749 ppm $CaCl_2$).

Formate concentration (% w/w)	Molar concentration (mol/L)	Density @ 50 °C (kg/m^3)	Viscosity @ 50 °C (cp)
5% formate solution	1.24	1112.0	1.03
15% formate solution	4.02	1206.0	1.73
20% formate solution	5.55	1249.5	2.32
29.6% formate solution	8.89	1352.5	5.17
32% formate solution	9.81	1379.5	6.34

Table 5
Densities and viscosities of formate solutions in brine at 75 °C. The brine had a total salinity of 102,646 ppm (97,897 ppm NaCl and 4749 ppm $CaCl_2$). At 75 °C, we observed precipitation of dissolved salts in solutions close to maximum solubility due to vaporization, because the holding cup of the rheometer was open to the atmosphere. Hence, we could not take reliable measurements for concentrations close to the maximum solubility at 75 °C.

Formate concentration (% w/w)	Molar concentration (mol/L)	Density @ 75 °C (kg/m^3)	Viscosity @ 75 °C (cp)
10% formate solution	2.57	1159.0	0.89
25% formate solution	7.25	1305.5	2.20
30% formate solution	9.03	1354.8	3.07

The case studies were based on numerical flow simulations of CO_2 injection and 30 wt% formate solution injection for two scenarios of geological carbon storage in a saline aquifer (Section 3.1) and an oil reservoir (Section 3.2) by using a multiphase compositional flow

simulator, CMG GEM [24]. Experimental data presented in Section 2 were used as part of the simulation input.

Sinomine Specialty Fluids [71] reported that formate brine compressibility values (in kPa^{-1}), $\frac{1}{\rho}\left(\frac{d\rho}{dP}\right)_T$, were of the order of 10^{-7} for temperatures between 0 and 250 °C, and pressures between 101 and 210,000 kPa. That is, a pressure change of 10,000 kPa would change the density by <1%. Additionally, Sinomine Specialty Fluids [72] estimated the pressure dependence of viscosity of a formate brine to be 0.52, 0.3, and 0.23 cp per 100,000 kPa at 38, 66, and 93 °C, respectively. The data showed a weak dependence of density and viscosity on pressure for the formate brine; hence, we assumed that the density and viscosity of the formate solution did not change with pressure in the simulation cases.

3.1. Case study 1. Saline aquifer

3.1.1. Numerical flow simulation

The simulation of carbon storage in an aquifer was based on the 3-D heterogeneous reservoir model presented in Sheng et al. [70]. The model used in this research was one of the stochastic realizations using sequential indicator simulation to represent two lithofacies (85 vol% clean sand and 15 vol% shale barriers) with each facies being homogenous and isotropic. The model has dimensions of 183 × 183 × 27 m^3 (600 × 600 × 90 ft^3) with a uniform gridblock size of 9 × 9 × 0.5 m^3 (30 × 30 × 1.5 ft^3) giving a total of 24,000 gridblocks. Fig. 4 shows the facies distribution of the 3-D aquifer model.

Table 6 gives the aquifer model properties. Both cases (CO_2 and aqueous formate solution) assumed a constant rate of carbon injection of 114 kmol of carbon (equivalent to 5 t of CO_2) per day. The reservoir pressure was controlled using a producer well, set to a pressure of 8963 kPa (1300 psia). Fig. 5 shows the relative permeability curves (only the one for water and gas was used in the simulations in this section).

The main difference between the CO_2 and formate cases lies in flow regime. In the CO_2 case, the injected CO_2 displaced the formation brine under the two-phase flow of gas and water with unstable displacement fronts and strong buoyant forces.

The stability of displacement fronts is typically evaluated by the endpoint mobility ratio (M^0) defined as

$$M^0 = \left(k^0_{rj}/\mu_j\right)/\left(k^0_{ri}/\mu_i\right)$$

where k^0_{ri} and k^0_{rj} are the endpoint relative permeabilities of the displaced and displacing fluids, respectively. μ_i and μ_j are the viscosities of the displaced and displacing fluids, respectively. M^0 greater than unity is considered unfavorable in that such displacement fronts tend to be unstable [5,32]. M^0 for the CO_2 case is calculated to be 6.4, in which i is the water phase and j is the gas phase. Since the formation brine and the formate solution are miscible, M^0 for the formate case reduces to the viscosity ratio, μ_i/μ_j, where μ_i and μ_j are the viscosities of the formation brine and the injected formate solution, respectively. That is, the viscosity ratio for the formate case is 0.13.

The relative significance of viscous to gravity forces in the displacement is captured by the gravity number, $\frac{N_{gv}M}{(1+M)}$, defined by Zhou

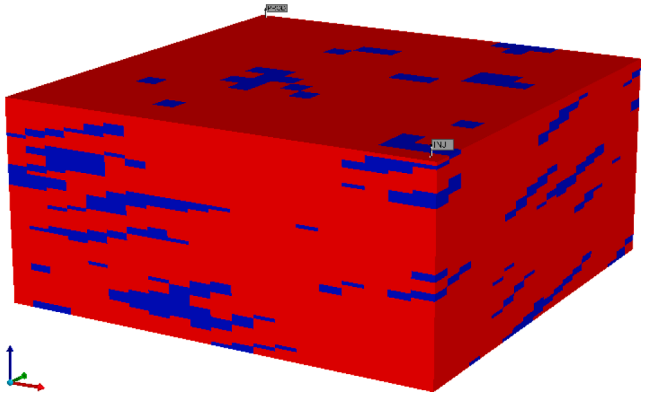

Fig. 4. 3-D aquifer model with two facies (Section 3.1). The sand facies are in red, and the shaly facies are in blue. The injector is at the bottom-right corner, and producer at the up-left corner. (For interpretation of the references to colour in this figure legend, the reader is referred to the web version of this article.)

Table 6
Properties used for the aquifer model in Case Study 1 (Section 3.1).

	Values
Reservoir properties	
Top depth	671 m (2200 ft)
Initial pressure	8963 kPa (1300 psia)
Temperature	41 °C (106 °F)
Initial water saturation	100%
Porosity	Sand – 0.33, Shale – 0.01
Permeability	Sand – 6500 mD, Shale – 1 mD
Fluid properties	
CO_2 density at initial aquifer temperature and pressure	400 kg/m^3 (25.17 lb./ft^3)
CO_2 viscosity at initial aquifer temperature and pressure	0.03 cp
Formate solution density	1400 kg/m^3 (87.4 lb./ft^3)
Formate solution viscosity	5 cp
Aquifer water density	1000 kg/m^3 (62.1 lb./ft^3)
Aquifer water viscosity	0.64 cp

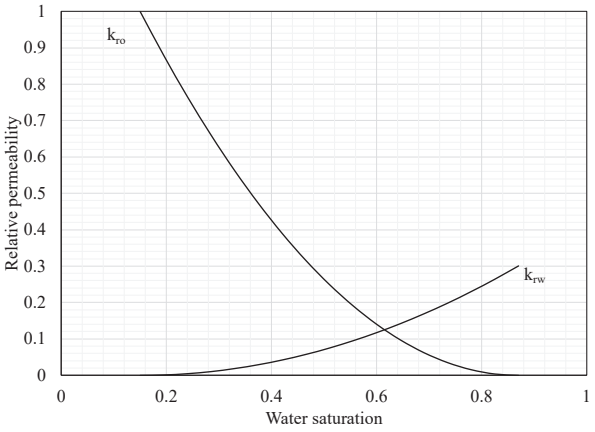

a. Water-oil relative permeability curves.

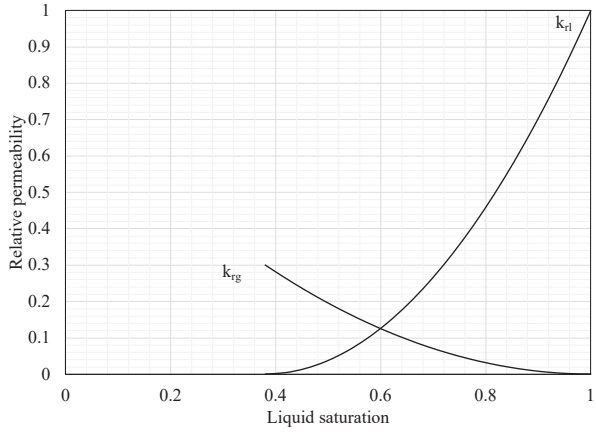

b. Liquid-gas relative permeability curves.

Fig. 5. Relative permeability curves used in the case studies (Sections 3.1 and 3.2).

et al. [82]. M is the mobility ratio, and N_{gv} is the characteristic time ratio for fluid to flow in the transverse direction due to gravity, defined as $N_{gv} = \frac{\Delta\rho g L k_{av}}{H u \mu_{brine}}$. $\Delta\rho$ is the density difference between the brine and injected fluid, g is acceleration due to gravity, L is the length of the aquifer, k_{av} is the average permeability in the vertical direction, H is the aquifer thickness, u is the Darcy velocity, and μ_{brine} is the viscosity of the brine. Gravity numbers >5 are indicative of gravity dominated flows [82]. Zhou et al.'s gravity number was calculated to be **16.77** for the CO_2 injection case and **71.77** for the formate injection case in this research. We used the sand permeability as the effective permeability, an average CO_2 density of 400 kg/m^3, endpoint mobility ratios, and an average pressure difference between the injection and producer wells of 17.65 kPa for the CO_2 case and 60.95 kPa for formate case based on simulation results.

The numerical simulation was performed for a simulated period of 34 years for the CO_2 and formate injection cases. Fig. 6 shows the profiles of gas saturation for the CO_2 case and the profiles of formate mole fraction in the aqueous phase for the formate case. The CO_2 case resulted in the gravity-dominant flow regime as indicated by the gravity number, in which the injected CO_2 accumulated from the top of the formation and displaced formation water with the immiscible gaseous CO_2 phase in the gravity-stable direction. The gravity-dominant flow regime was so strong that the displacement of water by CO_2, although immiscible, was not affected by the geological heterogeneity in the reservoir model used. The accumulation of CO_2 near the top of the formation indicates the potential leakage of gaseous CO_2 through hydraulic paths along any faults and wells to the surface.

The formate concentration profiles in Fig. 6 indicate the effects of gravity and the geological heterogeneity on the flow regime. However, the miscible displacement with a favorable viscosity ratio made the displacement fronts stable in the formate injection case.

Figs. 7, 8, and 9 respectively show the injectant (CO_2 or formate) production, cumulative water production, and cumulative carbon storage from the simulation. Each of CO_2 and formate contains one mole of carbon; hence, they are comparable on a carbon-mole basis. The CO_2 injection case exhibited the CO_2 breakthrough at 18 years (Fig. 7). Figs. 8 and 9 show that the water production and carbon storage leveled off upon the CO_2 breakthrough, resulting in a rapid reduction in the carbon-storage efficiency.

The favorable viscosity ratio in the miscible displacement in the formate injection case resulted in the water production (Fig. 8) that was not affected by the formate breakthrough at the producer. The carbon storage continued after the breakthrough in the formate case (Fig. 9). After 34 years of injection, the formate case resulted in 42% greater carbon stored (in moles) than the CO_2 case. The main difference between the two cases came from the carbon storage efficiency after the

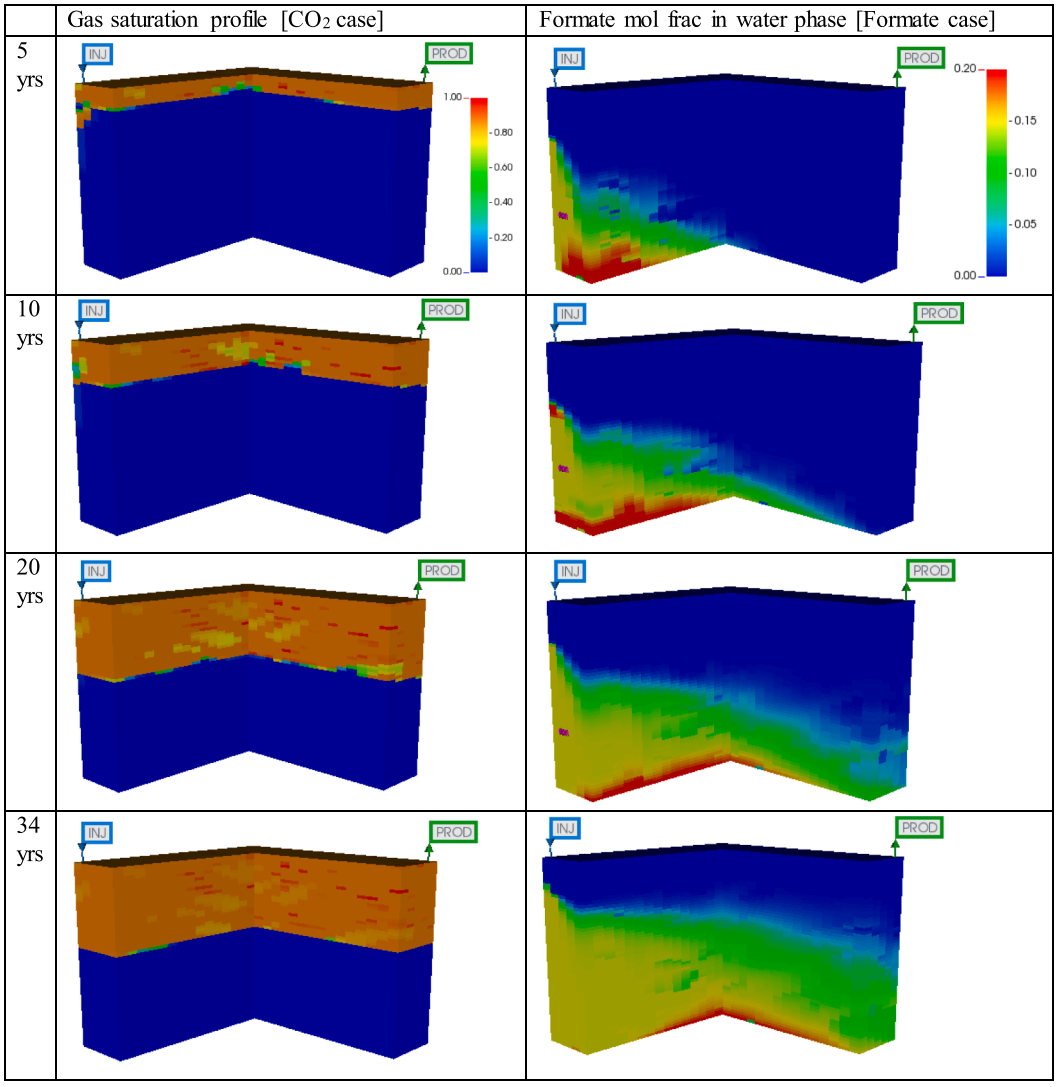

Fig. 6. CO_2 and formate distributions in aquifer over simulation period (Section 3.1). The CO_2 injection showed a clear gravity override profile, unlike the formate case. The profile developed into an even distribution of formate in the aquifer because the miscible displacement had a favorable viscosity ratio.

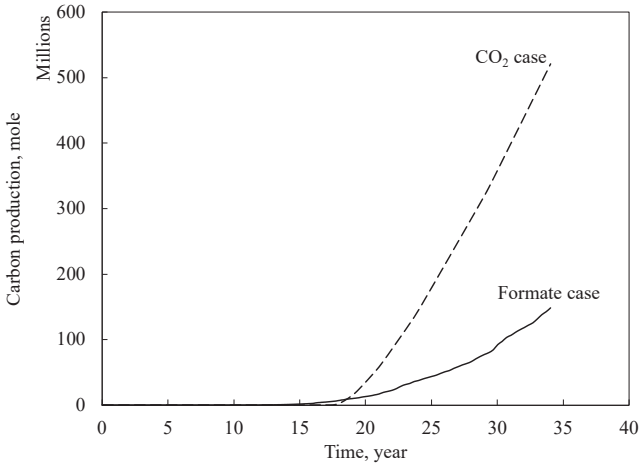

Fig. 7. Cumulative CO_2 and formate production from the aquifer in case study 1 (Section 3.1). Each molecule of formate and CO_2 contains one mole of carbon; hence, their production is comparable on a molar basis. The CO_2 production rose rapidly as soon as the CO_2 breakthrough began, which is typical of high-mobility gas. (For interpretation of the references to colour in this figure legend, the reader is referred to the web version of this article.)

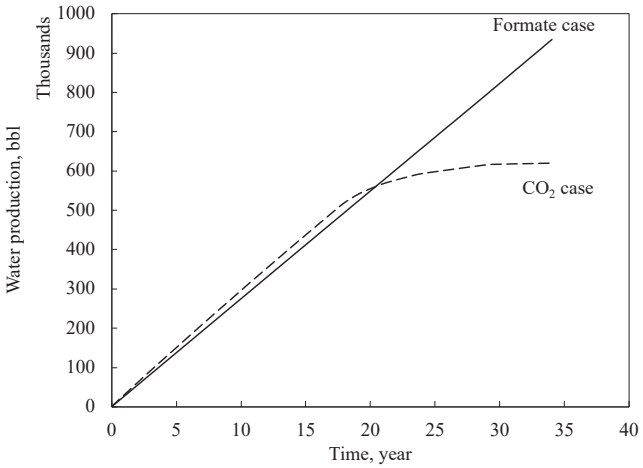

Fig. 8. Cumulative water production from the aquifer in case study 1. Once the CO_2 breakthrough happened, the water production leveled off. Almost all the CO_2 injected was produced after the breakthrough.

injectant's breakthrough.

This simulation case did not include the solubility of CO_2 in formation water and the subsequent geochemical reactions and diffusion of carbon species in the aqueous phase. CO_2 trapping via solubility, capillary, and mineralization is significant in geological CO_2 storage; however, these trapping mechanisms operate on different time scales. Capillary trapping, dissolution, and especially mineralization take place slowly, in hundreds to thousands of years, and do not contribute significantly during injection which is usually in decades [12,51,58,80]. Since the simulation was for the injection period that only spanned a few decades, we did not include CO_2 solubility in our simulations.

CO_2 dissolution in saline aquifers depends on the aquifer pressure, temperature, salinity of the formation water, and capillary pressure effects [54,81]. Zhang et al. [81] investigated the effect of capillary pressure on CO_2 solubility and stated that the CO_2 solubility was reduced by an average of 22% when capillary pressure effects on CO_2 solubility were considered. Hassanzadeh et al. [40] presented aquifer simulation results showing that <8% of the injected CO_2 would be trapped by dissolution in 200 years. Gupta et al. [39] presented CO_2 injection into aquifer simulation results showing that the fraction of CO_2 dissolved in the aqueous phase was between 4.5 and 6% during the period of injection and only rose to 8% after 500 years because the rate of dissolution slowed down considerably after injection.

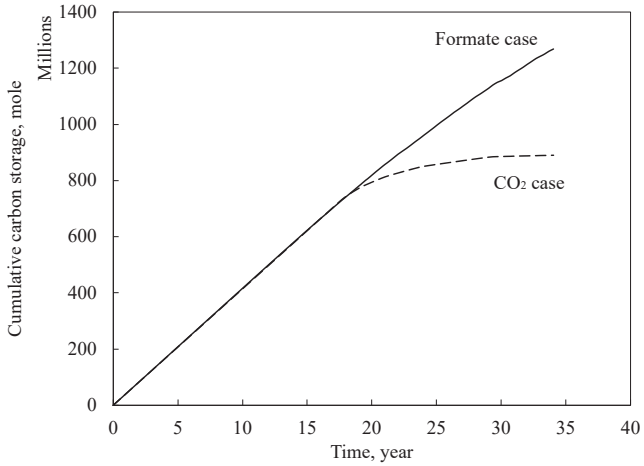

Fig. 9. Cumulative moles of the injectant stored in case study 1 (Section 3.1). The moles of formate stored increased steadily even after the breakthrough because the displacement of formation water by formate solution is miscible with a favorable viscosity ratio.

To quantify the possible contribution of dissolution to CO_2 storage in the aquifer case, we calculated the amount of CO_2 that could be dissolved in the aquifer after the injection period. At the end of the CO_2 injection, the mass of water left in the aquifer was 1.67×10^8 *kg*. In many cases, government regulations restrict CO_2 injection to aquifers with a certain salinity to protect potable water sources; for example, aquifers for CO_2 storage in the U.S. must contain brine with a salinity >10,000 ppm [80]. Hence, we assume that the aquifer contains 1 M NaCl brine, with a CO_2 solubility of 0.5 mol/kg water after capillary pressure adjustment [81]. The result shows the extra carbon storage due to dissolution would be about 9%, but this assumes complete mixing and does not consider the impact of reservoir heterogeneities on mixing between CO_2 and brine, nor the time scale for the dissolution.

Also, optimization of carbon storage for this case is possible with the elevations for the perforation zones of the injector and the producer. However, the important point to be made in this case study was the continued carbon storage even after the breakthrough in the formate injection case. The insensitivity of carbon storage to the breakthrough is expected to make the design of the geological carbon storage more robust under various uncertainties of geological formations.

3.1.2. *Cost-revenue analysis*

This subsection compares the costs and revenues of the two cases based on the financial model of Godec [36]. As mentioned previously, the objective is to indicate the cost of CO_2 ECR into formate, below which the formate injection case gives a greater NPV than the CO_2 injection case. The cost so calculated is referred to as "maximum allowable cost (MAC)" here.

Using the cost data in Godec [36], we created a model that includes the operation and maintenance costs, fluid lifting cost (for oil/water production), injection energy cost, transport cost, water treatment cost, and costs associated with the CO_2 recycle plant. The credit for carbon storage was the sole source of revenue in the financial model for this case study since there was no oil production, unlike in the next case study. The discount rate was set at 8%. Table 7 contains the model sections and description.

The following assumptions were made for the cost-revenue model:

Table 7
Inputs and their descriptions for the economic model used for case study 1 (Section 3.1).

	Description	Value
Cost		
Cost of CO_2	The cost of CO_2 gotten from a capture source is assigned a fixed cost of \$40/t-CO_2	\$40 × Total tonnes of CO_2 gotten from capture source
CO_2/ Formate transport cost	An estimate of \$0.06/t-mile [20]	\$0.06 × transport distance × tonnes of CO_2 transported
CO_2 recycle plant (CAPEX)	Capital cost associated with set up of a CO_2 recycle plant. It is based on peak CO_2 production.	\$1,200,000 × Peak CO_2 production (in MMcfd)
CO_2 recycle plant (O&M)	The operating costs (in \$ per Mcf of CO_2 recycled) associated with the recycle plant. This cost is set at 1% of oil price per barrel, because energy costs are a large part of the recycling process and produced oil is the energy source.	1% × Oil price × CO_2 produced
Annual O&M cost	Cost associated maintenance of well.	\$ (34,000 + 4D)/year, where D is the well depth (in feet)
Fluid lifting cost	Cost of energy required to lift fluids up a wellbore.	\$0.25 × Total fluid production (oil and water)
Liquid injection energy cost	Cost of energy required for water/formate injection.	\$0.08/bbl × bbls of liquid injected.
Water treatment cost	Cost associated with produced water management.	\$0.64/bbl × bbls of water produced
Revenue		
Oil sale revenue	Revenue from sale of produced oil. This is not present in aquifer case since there is no oil production.	\$60/bbl × bbls of oil produced
Carbon credit	Credit provided for storing carbon.	\$45/t-CO_2 × tonnes of CO_2 (or CO_2 equivalent in formate case) stored.

1. CO_2 was taken from a capture site and delivered to the injection site in its supercritical state and did not require a booster compression before injection; hence, the booster compression cost was not included in this research.
2. The injection used existing wells, pipelines, separators, and water treatment facilities. The only new equipment was a CO_2 recycling system as part of the capital expenditure. The cost of the CO_2 recycling system only affected the CO_2 injection case.
3. A cost of \$40 was assumed for each tonne of CO_2 taken from the capture site. This cost was assumed for the CO_2 injection case, but not the formate injection case; therefore, all CO_2 ECR costs estimated from this model are inclusive of CO_2 cost.
4. The oil price was \$60/bbl.
5. A credit of \$45 was received for each tonne of CO_2 stored. This was based on the U.S. Internal Revenue Code (IRC) Section 45Q [25].
6. Produced CO_2/formate solution was fully recycled, and the recycled injectant made up part of the subsequent injection. At a fixed carbon injection rate of 114 kmol/day, for example, if 114 kmol per day of CO_2 was produced, there would be no need to get CO_2 from the capture site as all the injected CO_2 would come from recycling, without incurring the cost of getting CO_2 from capture source.
7. Fixed costs for transportation – \$0.04/t-km (\$0.06/t-mile) [20], electricity - \$50/MWh.
8. The distance was 48.3 km (30 miles) from the capture site to the field injection site.

Fig. 10 shows that the NPV of the CO_2 injection case was negative all through the project; that is, the \$45/t-CO_2 carbon credit was not enough to cover the costs involved with the injection process. The revenue began to level off around 20 years when the cumulative carbon storage in the CO_2 case (Fig. 9) leveled off. Therefore, we calculated the breakeven carbon credit of \$86.82/t-CO_2 at 20 years. This is almost twice the assumed carbon credit based on the U.S. Internal Revenue Code (IRC) Section 45Q; however, the carbon credit is expected to increase in many countries [11,15,18,35,76,79].

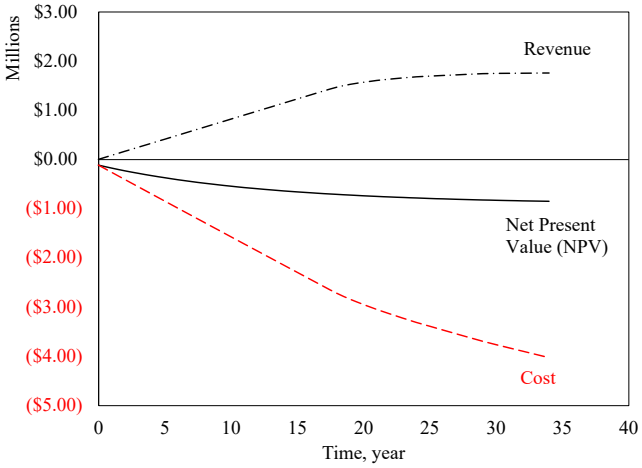

Fig. 10. Cashflows and net present value (NPV) over 34 years in case study 1 (Section 3.1). The NPV was gotten by applying an 8% discount rate to the nominal cash flows. The CCS project was not economically viable if the revenue source was only from the carbon credit of \$45 per tonne of CO_2 stored.

Table 8 shows the total discounted cost and revenue for both CO_2 and formate injection cases after 20 years of injection. Using the breakeven carbon credit (\$86.82/t-CO_2), we calculated the MAC for CO_2 ECR to be \$46/t-CO_2 at 20 years. Over the 20 years of injection, both CO_2 and formate injection cases gave nearly the same carbon storage as shown in Fig. 9; therefore, the 12% difference between the MAC for formate and the price of CO_2 was solely because the formate case did not need the CO_2 recycling plant. This economic analysis did not include the upside potential of carbon storage by formate solution that was shown in later years; that is, the MAC for formate presented above is a conservative estimation with the same carbon storage as the CO_2 injection case.

3.2. Case study 2. Oil reservoir (EOR and carbon storage)

The IEA [45] reported that the injection of CO_2 for enhanced oil recovery (CO_2 EOR) is the second-largest use of CO_2. This subsection compares the CO_2 injection and formate injection cases in an oil reservoir.

Table 8
Discounted costs and revenue for the CO_2 and formate case accrued over 20 years of injection in case study 1 (Section 3.1). The cost values are considered negative and put in brackets "()" to connote that.

	Amount
CO_2 injection case	
Cost of CO_2	\$ (703,771.70)
Transport cost	\$ (31,669.73)
Recycle cost $^{CAPEX+OPEX}$	\$ (117,993.65)
O&M cost	\$ (423,162.15)
Fluid lifting cost	\$ (70,482.40)
Water treatment cost	\$ (180,434.95)
Carbon credit	\$ 791,743.17
Formate injection case	
Transport cost	\$ (32,145.42)
Recycle/Water treatment cost	\$ (172,768.26)
O&M cost	\$ (423,162.15)
Fluid lifting cost	\$ (67,487.60)
Liquid-injection energy cost	\$ (21,716.36)
Carbon credit	\$ 785,641.18

3.2.1. Numerical flow simulation

The reservoir model was based on the heterogeneous sandstone reservoir model from the tenth SPE comparative solution project [23]. The original model had dimensions 366 × 671 × 52 m^3 (1200 × 2200 × 170 ft^3) and a uniform gridblock size of 6 × 3 × 0.6 m^3 (20 × 10 × 2 ft^3) resulting in 1.122 × 10^6 gridblocks. The current study used a 122 × 122 × 21 m^3 (400 × 400 × 70 ft^3) section from the Tarbert formation, which is a shallow marine sandstone with fine to medium-sized grains sandstones and some thin layers of siltstones and shales [33]. The simulation used a quarter of a five-spot pattern (an injection pattern in which four injection wells are located at the corners of a square and the production well sits in the center). The uniform gridblock size dimensions of 6 × 3 × 0.6 m^3 (20 × 10 × 2 ft^3) resulted in 20 × 40 × 35 (28,000) gridblocks. Fig. 11 shows a 3-D view of the reservoir porosity distribution.

Table 9 gives the properties of the selected reservoir section. The model used by Christie and Blunt [23] was originally generated for use in the PUNQ (Production Forecasting with Uncertainty Quantification) project, an investigation into history matching and uncertainty quantification. The original PUNQ model used a uniform value of the ratio of vertical permeability to horizontal permeability (k_v/k_h) across the whole model as in the simulation in this section; however, k_v/k_h was set to 0.3 in the fracture and 0.0001 for the matrix in the tenth SPE comparative solution project [23], as will be used as a sensitivity test in Section 3.2.4. Table 10 shows the oil composition and fluid properties used for this simulation case.

For both cases (CO_2 and aqueous formate solution), oil production was initiated by five years of waterflooding at 11,376 kPa (1650 psia). After that, both injections were set at a constant rate of 114 kmol of carbon per day (equivalent to 5 t of CO_2 per day). The production pressure was kept at 10,342 kPa (1500 psia). The phase behavior was modeled by the Peng-Robinson equation of state. The thermodynamic minimum miscibility pressure for CO_2 with the oil (oil composition given in Table 2) was calculated to be 10,053 kPa (1458 psia) at the reservoir temperature, 41 °C (106 °F), using the equation-of-state model. We measured the oil/aqueous interfacial tension (IFT) for brine and a 30 wt% formate in brine solution to be 10.16 and 3.23 mN/m, respectively. Amaefule and Handy [9] studied the effect of IFT on oil/water relative permeability and found that the relative permeability did not change significantly above 0.1 mN/m. Since the measured IFT values for the brine and the formate solution are much >0.1 mN/m, we assumed the relative permeability of oil and water to be the same as that of oil and formate solution. Fig. 5 shows the 2-phase relative permeability curves used in the simulation. The 3-phase relative permeability was generated using Stone's model II. The simulations for the two cases were performed for a simulated period of 40 years, including the initial water flooding for five years.

Table 9
Properties of the reservoir section used for Case Study 2 (Section 3.2).

Reservoir properties	
Top depth	671 m (2,200 ft)
Initial pressure	10,342 kPa (1500 psia)
Temperature	41 °C (106 °F)
OOIP	46,800 m^3 (294,365 bbl)
Initial oil saturation	85%
Initial water saturation	15%
Porosity	0 to 0.50
Horizontal permeability	0 to 20 D
Vertical to horizontal permeability (k_v/k_h) ratio	0.3
Residual water saturation	15%

Unlike in case study 1, the injection into an oil reservoir involves the multiphase displacements of oil and formation water by the injection fluid. The main difference between the CO_2 and formate injection cases came from the flow regime affected strongly by the stability of the displacement processes and buoyant forces; however, these two factors appeared differently from the previous case study because of the strong tendency of channeling flow through fracture networks.

M^0 for the injectant and oil was calculated to be 13 for the CO_2 case, and 0.16 for the formate case. M^0 for the injectant and formation water was calculated to be 3.1 for the CO_2 case. The displacement of formation water by formate solution was a miscible process with a favorable viscosity ratio, 0.13.

Fig. 12 presents the profiles of the overall CO_2 mole fraction for the CO_2 injection case and the formate mole fraction in the aqueous phase for the formation injection case at different times. Figs. 13, 14, 15, and 16 show the water production, oil production, injectant storage, and average reservoir pressure results from the simulations. The CO_2 case showed a gravity override and the injected CO_2 preferentially displaced oil more than formation water because of the M^0 values presented above. The formate injection case showed a stable propagation of displacement fronts with no gravity-driven flow and efficient displacement of water and oil phases even after the breakthrough. The formate injection resulted in 15% greater oil recovery and 37% greater carbon stored than the CO_2 injection case.

The average reservoir pressure declined slowly in the CO_2 case, while the formate injection caused a significant increase in the reservoir pressure. This increase in pressure by the formate injection in comparison to CO_2 can be attributed to the difference in volumetric flow rates and the fluid compressibility between both cases. Though the simulations were performed using a constant molar rate of carbon, 114 kmol/

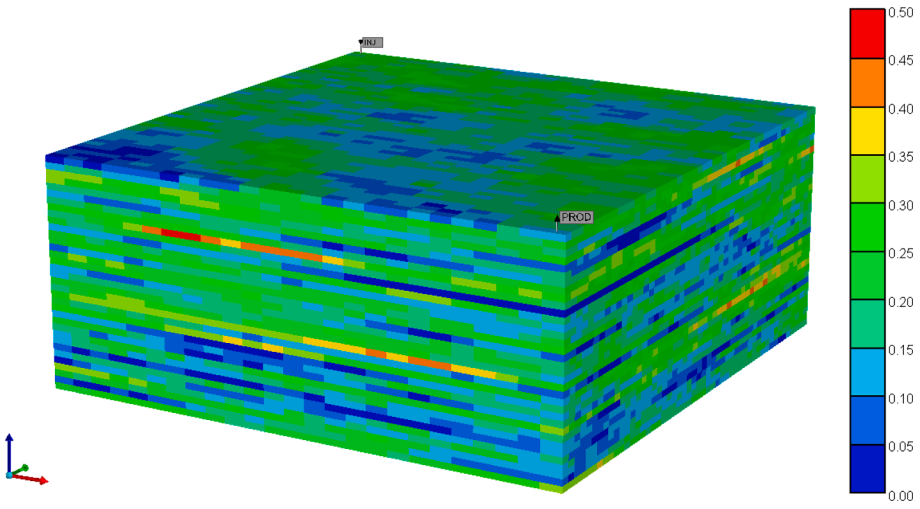

Fig. 11. 3-D view of the reservoir porosity distribution; taken from the tenth SPE comparative solution project [23]. The colour scale indicates porosity.

Table 10
Oil composition and fluid properties used for case study 2 (Section 3.2). "PC" stands for pseudocomponent, and four PCs represent the C_{7+} fraction of the oil.

Oil composition. Kumar [50]	Mole percent	Molecular weight (g/mol)
N_2	0.5%	
CO_2	0.4%	
CH_4	12.7%	
C_2H_6	6.7%	
C_3H_8	6.9%	
n-C_4H_{10}	6.2%	
n-C_5H_{12}	5.2%	
n-C_6H_{14}	2.9%	
PC-1	24.2%	136.83
PC-2	15.9%	207.56
PC-3	11.4%	291.23
PC-4	7.1%	467.50
Oil properties		
Viscosity	2.61 cp	
Density	806 kg/m^3 (44°API)	
Bubble point	5599 kPa (812 psia)	
Fluid properties		
CO_2 density at initial reservoir conditions	560 kg/m^3 (34.78 lb./ft^3)	
CO_2 viscosity at initial reservoir conditions	0.062 cp	
Formate solution density	1400 kg/m^3 (87.4 lb./ft^3)	
Formate solution viscosity	5 cp	
Aquifer water density	1000 kg/m^3 (62.1 lb./ft^3)	
Aquifer water viscosity	0.64 cp	

day, the volumetric flow rate differed in each case. For the CO_2 case, assuming a density of 600 kg/m^3 based on the initial reservoir conditions, the volumetric flow rate was 8.3 m^3 per day. In the formate injection case, using a formate concentration of 30 wt% and density of 1400 kg/m^3, the volumetric flow rate was 11.9 m^3 per day. The compressibility of supercritical CO_2 is in the order of 10^{-5} kPa^{-1}, which is about two orders of magnitude greater than the formate solution compressibility and typical rock compressibility [52,74]. When CO_2 is injected into the formation, it displaces some of the water and oil in the formation, and since it is relatively more compressible than the displaced fluids it does not create a noticeable increase in pressure. The formate solution is only slightly incompressible, and with its continued injection, it replaces the more compressible oil causing a significant change in the average reservoir pressure. This compressibility difference coupled with the increased volumetric flow rate for the formate case contributed to the increased pressures shown in Fig. 16. For carbon storage, large pressure increases are undesirable because of the need to avoid fracturing the formation. For a CO_2-like pressure profile at the same molar carbon injection rate, the formate injection might require additional production wells to adjust for the increased volumetric flow rate.

With the increased oil recovery, there might be concerns about formate giving off more carbon emissions. We calculated the mole numbers of produced hydrocarbon components in the oil, summed up the number of carbon molecules produced, and compared it to the number of carbon molecules stored, to see how much reduction in carbon intensity was achieved by each injectant. In 15 years of injecting CO_2/formate, the formate case resulted in a 20% reduction in carbon intensity while the CO_2 case resulted in a 16% carbon intensity reduction as shown in Fig. 17. That is, the larger injectant storage makes up for the higher oil recovery gotten from the formate case. The results suggest that the carbon storage in an oil reservoir requires a deliberate design for not only the efficient displacement of oil, but also the efficient displacement of water (water from water flooding and connate water).

3.2.2. Cost-revenue analysis

The cost-revenue analysis was performed by using the simulation results and the financial model described in the previous subsection with the addition of revenue from oil sales. This oil reservoir injection scenario did not consider the first five years of oil production by waterflooding; that is, the focus was on the CO_2 and formate injection periods. The capital cost of the CO_2 recycling plant was accounted for in year 5.

Fig. 18 shows the cumulative cost, revenue, and NPV of the CO_2 injection project over 35 years of CO_2/formate injection (only for a quarter of the five-spot pattern). Unlike in case study 1, the NPV of the CO_2 injection case was positive because of the revenue from oil sales.

The CO_2 case yielded an NPV of $2.6 million from a quarter of the five-spot pattern after 20 years, before leveling off. Since the cost of CO_2 ECR into formate is uncertain, we compared the cash flows from both cases and solved for the following cost parameters: the equivalent formate cost and the breakeven formate cost. The equivalent formate cost is the estimated cost of formate that would give the same NPV as the CO_2 case; the breakeven formate cost is the estimated cost that would give a zero NPV for the formate injection case as a standalone project. These parameters give a rough estimate of probable costs for the research and development of CO_2 ECR systems.

Fig. 19 shows the equivalent and breakeven costs of formate calculated. By Year 20, the equivalent cost was $269/t-$CO_2$ and the breakeven cost was $575/t-$CO_2$. That is, the formate injection case can give a similar NPV to the CO_2 injection case even when CO_2 ECR into formate takes $269/t-$CO_2$. Somoza-Tornos et al. [73] showed in their review article that production costs of formic acid via CO_2 ECR ranged from $100 to $2630/t-$CO_2$. As in Somoza-Tornos et al. [73], the equivalent and breakeven costs calculated in this research include CO_2 cost in addition to electrolyzer electricity cost, and operation/capital costs. In terms of production cost per tonne of CO_2, therefore, CO_2 ECR can be an economically viable option for the scenario studied in this section. Lee et al. [53] in their review on electrochemical CO_2 reduction reported CO_2 throughputs in some pilot-scale CO_2 ECR plants, with the values ranging from 0.4 to 36.5 t per year. Therefore, it would be more practical to start implemeting CO_2 ECR for carbon sequestration for distributed small-scale projects. Since typical CO_2 CCS projects have CO_2 injection rates ranging from 1 to 4.8 million tonnes per year [42], increasing the throughput of CO_2 ECR will be an important research task.

3.2.3. Sensitivity analysis using economic parameters

The major parameters of the financial model were adjusted to see the effect of changing these parameters on the NPV for the CO_2 case. The four parameters adjusted were oil price, discount rate, CO_2 cost, and carbon credit. These values were adjusted by ±40%. Table 11 contains the base and adjusted values of the economic parameters considered.

Fig. 20 is a tornado plot showing the effects of the changing model parameters on the CO_2 case NPV. The tornado plot shows that oil price and discount rate were the most impactful parameters. Looking at the aquifer case (section 3.1) and the NPV based on the 45Q tax credit, the revenue from oil sales was the key to the economic viability in case study 2. The tornado plot further shows that changes in oil price would be a key determinant of the economic viability in this case study. The discount rate often correlates with the maximum allowable risk for the project, and it is dependent on the operator. The impact of carbon credit and CO_2 cost were relatively low because the bulk of the revenue was from oil sales, and because the CO_2 purchase cost reduced greatly with CO_2 production (breakthrough), leading to recycling of the produced CO_2.

3.2.4. Sensitivity analysis on k_v/k_h

The k_v/k_h value for the matrix was adjusted from 0.3 (Section 3.2.1) to 0.0001 while keeping the k_v/k_h value of 0.3 for the fracture volumes. As described previously, this corresponds to the setting in the tenth SPE

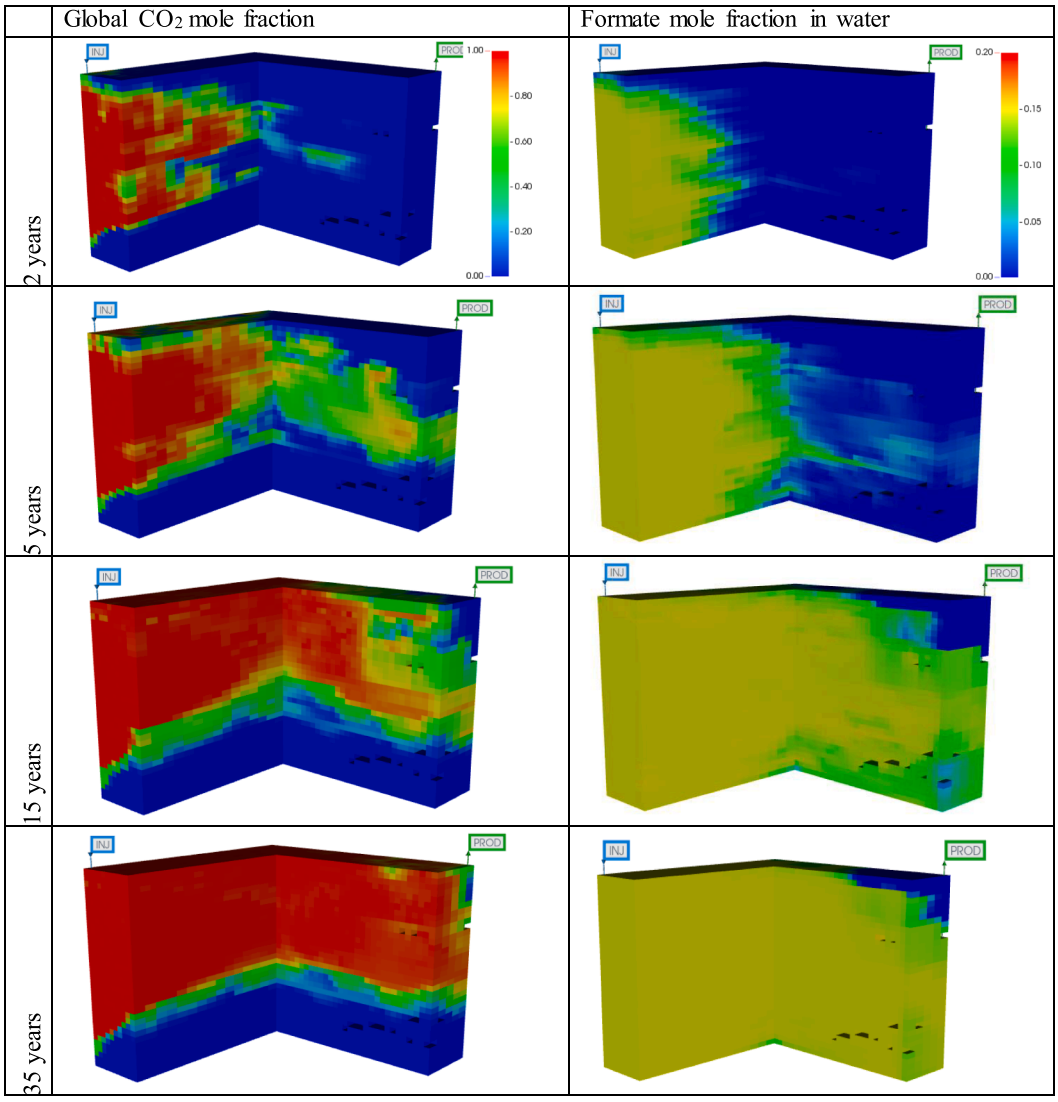

Fig. 12. Profiles of CO_2 and formate at different times in case study 2 (Section 3.2). The timeframe in the first column refers to the time after the start of CO_2/formate injection. Oil production was initiated by 5 years of waterflooding. The formate injection case shows stable displacement fronts and a more efficient displacement of oil and water than CO_2.

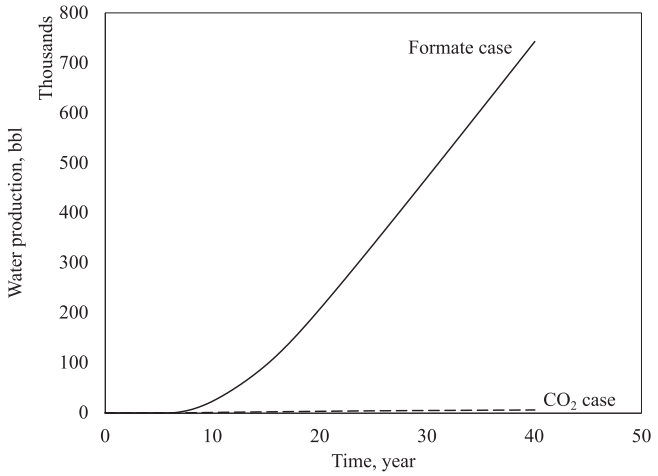

Fig. 13. Cumulative water production simulated in case study 2 (Section 3.2).

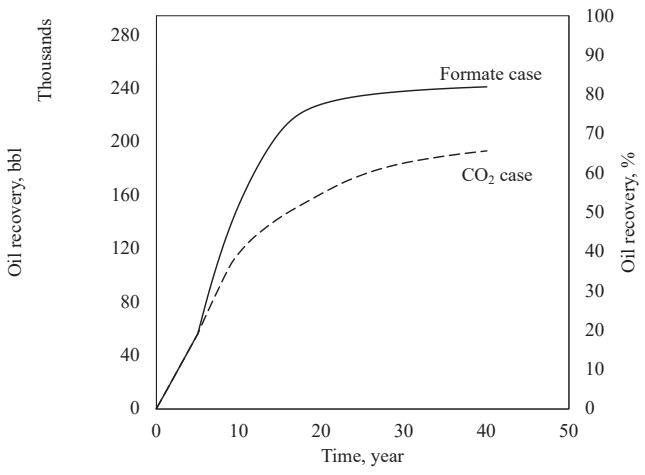

Fig. 14. Oil recovery from the CO_2 and formate solution injection in case study 2 (Section 3.2). The formate injection case resulted in approximately 20% more oil recovery than the CO_2 injection case.

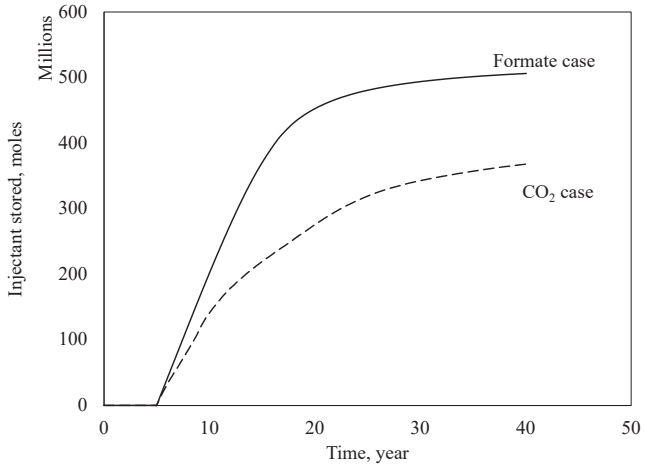

Fig. 15. Histories of the moles of the injectant stored in case study 2 (Section 3.2). One mole of CO_2/formate contains one mole of carbon; hence, the moles of CO_2/formate stored are equivalent to the moles of carbon stored.

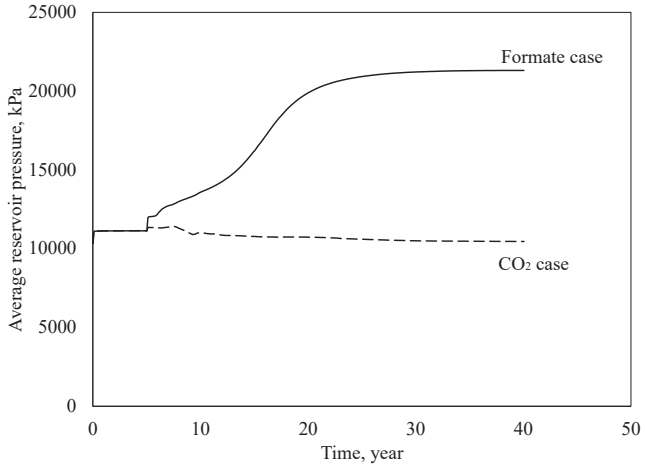

Fig. 16. Average reservoir pressure histories from the CO_2 and formate solution injection in case study 2 (Section 3.2).

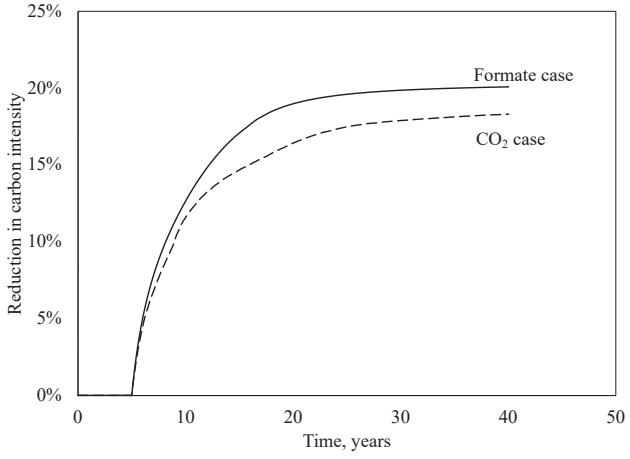

Fig. 17. Reduction in carbon intensity. This is the ratio of the moles of carbon in the injectant stored to the moles of carbon in the oil produced by the injectant. Though the formate injection produced more hydrocarbons (oil) than the CO_2 injection, the formate still gave a higher reduction in carbon intensity compared to CO_2.

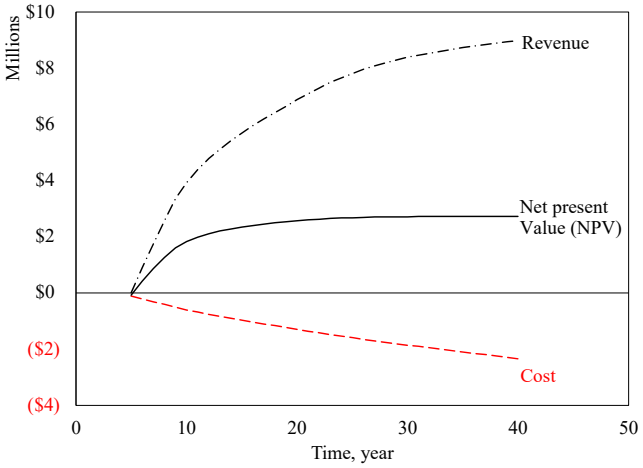

Fig. 18. Cashflows and net present value (NPV) of CO_2 injection into oil reservoir. Oil production was initiated by 5 years of waterflooding. With the focus being on the CO_2/Formate injection the financial analysis only considers the period of CO_2 injection which started in Year 6.

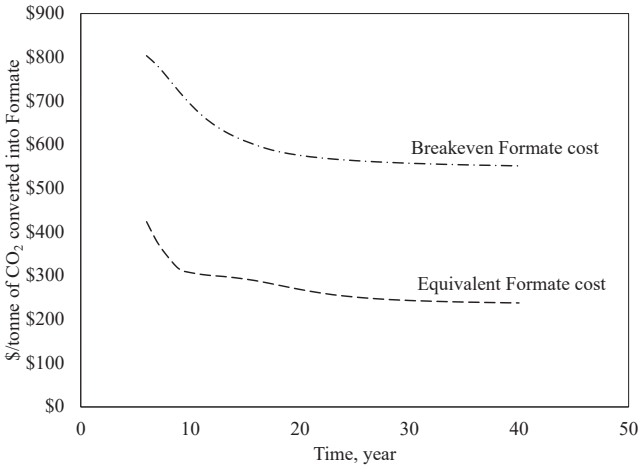

Fig. 19. Equivalent and breakeven formate costs for CO_2 ECR into formate. The equivalent formate cost is the cost of formate that would give the same NPV as the CO_2 injection case at a particular year. When the NPV for the CO_2 injection case leveled off after 20 years, the equivalent formate cost was $269/t-$CO_2$.

Table 11
The adjusted economic parameters, the base values and the ±40% values for a sensitivity analysis of case study 2 (Section 3.2.3).

	Base values	+40%	−40%
Oil price	$60 per barrel of oil	$84 per barrel of oil	$36 per barrel of oil
Discount rate	8%	11.2%	4.8%
CO_2 cost	$40 per tonne of CO_2	$56 per tonne of CO_2	$24 per tonne of CO_2
Carbon credit	$45 per tonne of CO_2 stored	$63 per tonne of CO_2 stored	$27 per tonne of CO_2 stored

comparative solution project [23]. The effects of the change in k_v/k_h on flow patterns, carbon storage, and oil recovery for the CO_2 and formate injection cases were examined.

The change in k_v/k_h had a significant effect on the observed injectant distribution profile, as shown in Fig. 21. The substantial reduction in k_v/k_h resulted in the increased level of channeling flow, and therefore, suppression of the gravity-driven flux as can be seen especially in the CO_2 case. Figs. 22 and 23 show the oil production and carbon storage for

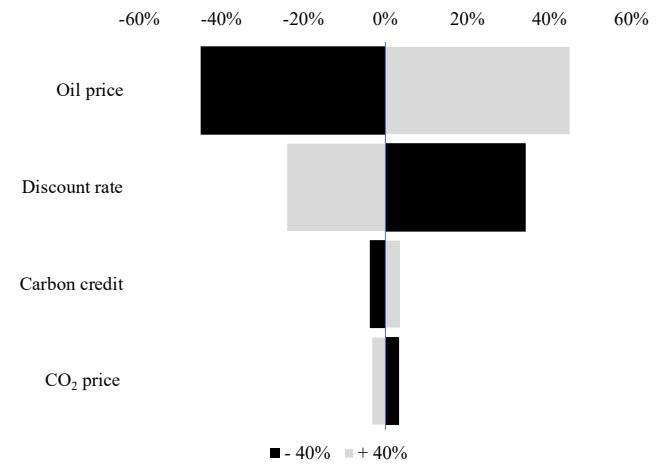

Fig. 20. Sensitivity of CO_2-EOR NPV to changes in oil price, discount rate, carbon credit, and CO_2 cost (at 20 years) in case study 2 (Section 3.2.3). The black boxes represent a − 40% change in the parameter's base value, while the grey boxes represent a + 40% change.

both reservoir settings (k_v/k_h = 0.3 and 0.0001). There was a reduction in oil and carbon storage with the significantly reduced k_v/k_h for both cases; however, the CO_2 case was much more affected by this adjustment. The oil recovery was reduced by 50% and carbon storage by 52% in the CO_2 injection case while the oil recovery was reduced by 25% and carbon storage was reduced by 19% in the formate injection case.

This sensitivity analysis indicates a substantial advantage of using formate as a carbon carrier for controlling the risk of CCS associated with the permeability heterogeneities and their impact on subsurface flow regime. Previous studies on using formate brine as the base fluid in drilling muds showed that aqueous formate solutions were compatible with polymers and retained the stability at temperatures as high as 150 °C; hence, it is practically possible to control the in-situ flow regime for formate (the carbon carrier) by adjusting the density and viscosity of the formate solution injected [27,29,43,59].

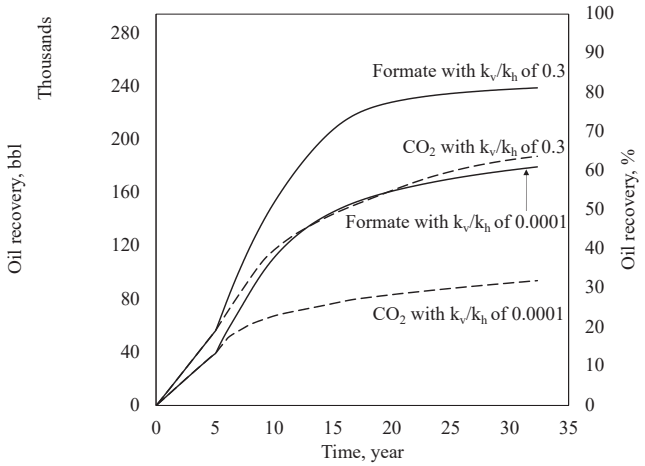

Fig. 22. Oil production results for the CO_2 and formate injection cases in case study 2, using the k_v/k_h value of 0.3 and 0.0001.

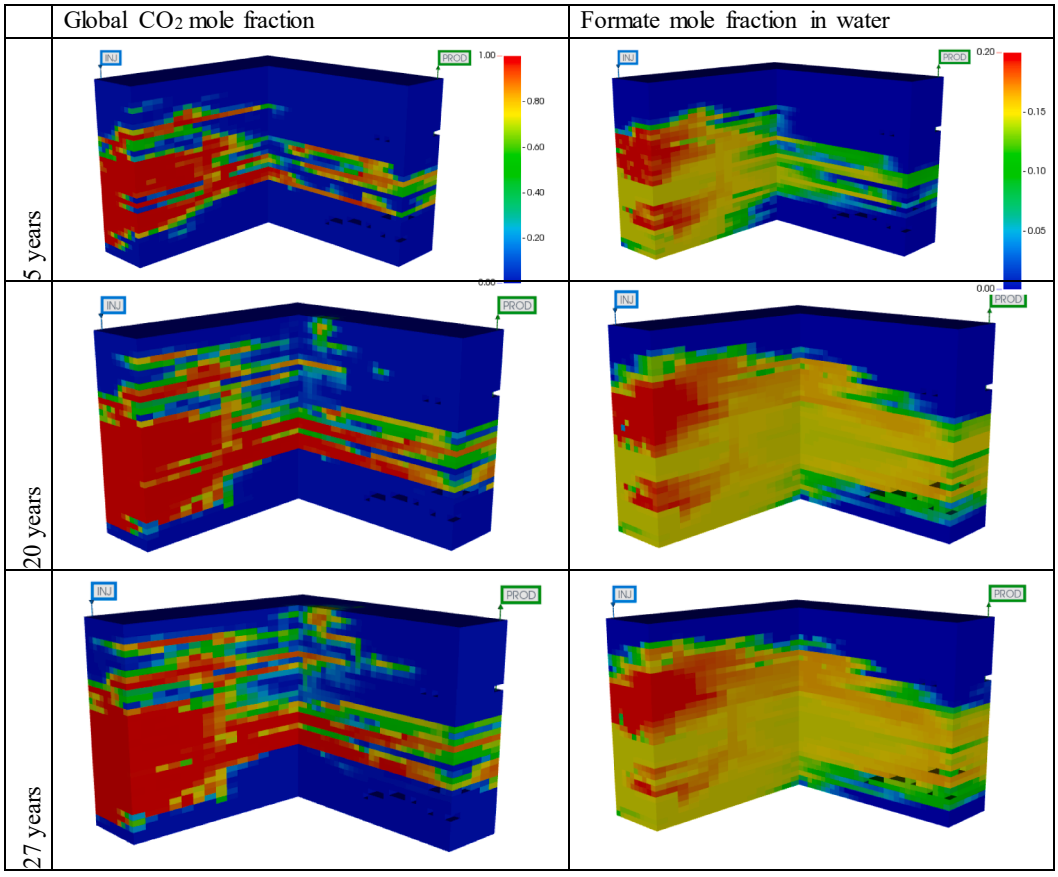

Fig. 21. Profiles of CO_2 and formate in the oil reservoir using an adjusted k_v/k_h value of 0.0001 for the matrix volume [23]. The timeframe in the first column refer to the time after the start of CO_2/formate injection.

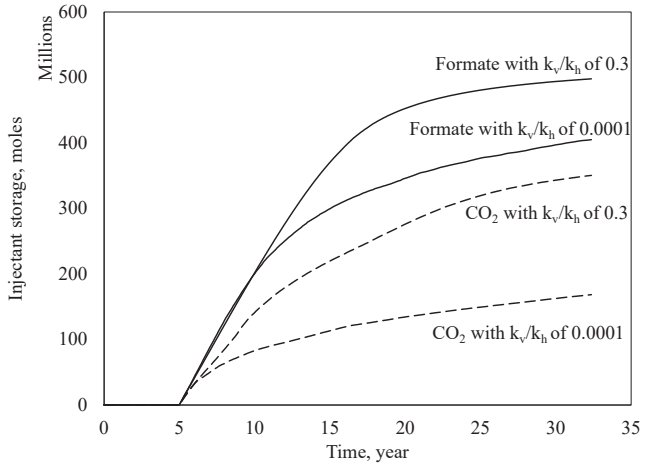

Fig. 23. Injectant storage for the CO_2 and formate injection cases in case study 2, using the k_v/k_h value of 0.3 and 0.0001.

4. Conclusions

This paper presented case studies of aqueous formate solution as a carbon carrier for geological carbon storage in comparison to CO_2 as the conventional carbon carrier. New experimental data were reported for properties of formate solutions in brines and used to set up numerical flow simulation for the case studies. The main objective of the case studies was to indicate the allowable cost of CO_2 ECR for geological carbon storage using aqueous formate with a comparable NPV with the CO_2 injection case. The main conclusions are as follows:

- Experimental data showed that formate is stable in NaCl+$CaCl_2$ brine (102,600 ppm), with the formate solubility ranging from 30 wt % to 35 wt% at temperatures between 25 and 75 °C.
- Newtonian behavior was consistently observed for the formate solutions in the brine at different formate concentrations and temperatures. The measured viscosities were well correlated as a logarithmic function of the molar concentration of formate. Viscosities of 30 wt% formate solutions in the 102,600-ppm brine were approximately 12 cp at 25 °C, 5 cp at 50 °C, and 3 cp at 75 °C.
- Two simulation case studies of carbon storage were performed: case study 1 for an aquifer and 2 for an oil reservoir. For each case study, CO_2 and formate injection were compared in terms of flow regime and displacement of reservoir fluids (formation water in case study 1 and formation water and oil in case study 2). Although the flow regimes depended on reservoir properties, the formate injection case showed much more stable fronts of oil and water displacement. The more stable fronts yielded the oil recovery and the carbon storage that were insensitive to the injectant breakthrough. In all studied scenarios, the formate solution injection case resulted in approximately 40% larger carbon (in moles) storage in comparison to the CO_2 injection case.
- The formate injection simulations showed no upward buoyancy-driven flux, unlike the CO_2 injection simulations. The flow profiles developed in the simulations showed channeling in heterogeneous reservoirs for the CO_2 injection cases. Such unfavorable flow patterns were suppressed by more stable displacement fronts in the formate injection.
- Cost-revenue analysis showed that the economic viability of carbon storage in an aquifer would depend so much on the value of carbon credit. The carbon credit value of \$87/t-CO_2 was necessary for the CO_2 injection case to have zero NPV for carbon storage in the aquifer model studied in this research. With this hypothetical carbon credit value, the maximum allowable cost for CO_2 ECR was \$46/t-CO_2.
- The case study of EOR and carbon storage in an oil reservoir showed that the NPV of the formate injection case would be equivalent to that of the CO_2 injection case when the cost of CO_2 ECR into formate was \$269/t-CO_2 for year 20 and \$238/t-CO_2 for Year 40. The breakeven cost of CO_2 ECR for the formate injection case was \$575/t-CO_2 for Year 20 and \$551/t-CO_2 for Year 34.
- Although these estimated range of CO_2 ECR costs are sensitive to oil price, discount rate, and reservoir properties among many other factors, they are not unrealistically higher than the current costs of CO_2 ECR as reported in Somoza-Tornos et al. [73]. Results in this research support the necessity of research and development for efficient CO_2 ECR systems.

Nomenclature

% w/w	percent weight by weight
-ppm	parts per million
μ	Viscosity
y	Concentration of formate in solution, mol/dm^3
ρ	Density
k_r^0	Endpoint relative permeability
k_h	Horizontal permeability
k_v	Vertical permeability
M^0	Endpoint mobility ratio
N_{gv}	Characteristic time ratio for fluid to flow in the transverse direction due to gravity
t	tonne
M	Mobility ratio

Abbreviations

CCS	Carbon capture and storage
CCUS	Carbon capture, utilization, and storage
CO2 ECR	CO2 electrochemical reduction
DIW	Deionized water
EOR	Enhanced Oil Recovery
IFT	Interfacial tension
M	Mobility ratio
MAC	Maximum allowable cost
NPV	Net present value
OOIP	Original oil in place
PC	Pseudocomponent
PUNQ	Production Forecasting with Uncertainty Quantification
SPE	Society of Petroleum Engineers
TRL	Technology Readiness Level

CRediT authorship contribution statement

Oluwafemi Precious Oyenowo: Validation, Formal analysis, Investigation, Data curation, Writing – original draft, Visualization. **Kai Sheng:** Methodology, Validation, Formal analysis, Investigation, Data curation, Visualization. **Ryosuke Okuno:** Conceptualization, Methodology, Validation, Formal analysis, Resources, Writing – original draft, Writing – review & editing, Supervision, Project administration, Funding acquisition.

Declaration of Competing Interest

The authors declare that they have no known competing financial interests or personal relationships that could have appeared to influence the work reported in this paper.

Data availability

Data will be made available on request.

Acknowledgements

We acknowledge sponsors of the Energi Simulation Industrial Affiliate Program on Carbon Utilization and Storage at the Center for Subsurface Energy and the Environment at the University of Texas at Austin. Ryosuke Okuno holds the Pioneer Corporation Faculty Fellowship in Petroleum Engineering at the University of Texas at Austin.

References

[1] IPCC. Summary for policymakers. In: MassonDelmotte V, Zhai P, Pirani A, Connors SL, Péan C, Berger S, et al., editors. Climate change 2021: the physical science basis. Contribution of working group I to the sixth assessment report of the intergovernmental panel on climate change. Cambridge University Press; 2021.
[2] Celia MA, Bachu S, Nordbotten JM, Bandilla KW. Status of CO_2 storage in deep saline aquifers with emphasis on modeling approaches and practical simulations. Water Resour Res 2015;51(9):6846–92. https://doi.org/10.1002/2015wr017609.
[3] IPCC. IPCC special report on carbon dioxide capture and storage. In: Metz B, Davidson O, de Coninck HC, Loos M, Meyer LA, editors. Prepared by working group III of the intergovernmental panel on climate change. Cambridge, United Kingdom and New York, NY, USA: Cambridge University Press; 2005. p. 442.
[4] Kelemen P, Benson S, Pilorgé H, Psarras P, Wilcox J. An overview of the status and challenges of CO_2 storage in minerals and geological formations. Front Clim 2019; 1. https://doi.org/10.3389/fclim.2019.00009.
[5] Ahmed T, Meehan DN. Introduction to enhanced oil recovery. In: Advanced reservoir management and engineering. 2nd ed. Gulf Professional Publishing; 2012. p. 541–85. https://doi.org/10.1016/B978-0-12-385548-0.00006-3.
[6] Ajayi T, Gomes JS, Bera A. A review of CO_2 storage in geological formations emphasizing modeling, monitoring and capacity estimation approaches. Pet Sci 2019;16:1028–63. https://doi.org/10.1007/s12182-019-0340-8.
[7] Al-Mamoori A, Krishnamurthy A, Rownaghi AA, Rezaei F. Carbon capture and utilization update. Energ Technol 2017;5(6):834–49. https://doi.org/10.1002/ente.201600747.
[8] Al-Tamreh SA, Ibrahim MH, El-Naas MH, Vaes J, Pant D, Benamor A, et al. Electroreduction of carbon dioxide into formate: a comprehensive review. ChemElectroChem 2021;8(17):3207–20. https://doi.org/10.1002/celc.202100438.
[9] Amaefule JO, Handy LL. The effect of interfacial tensions on relative oil/water permeabilities of consolidated porous media. Soc Petrol Eng J 1982;22(03): 371–81. https://doi.org/10.2118/9783-PA.
[10] Aminu MD, Nabavi SA, Rochelle CA, Manovic V. A review of developments in carbon dioxide storage. Appl Energy 2017;208:1389–419. https://doi.org/10.1016/j.apenergy.2017.09.015.
[11] Anderson JJ, Rode D, Zhai H, Fischbeck P. A techno-economic assessment of-carbon-sequestration tax incentives in the US power sector. Int J Greenhouse Gas Control 2021;111:103450. https://doi.org/10.1016/j.ijggc.2021.103450.
[12] Bachu S, Bonijoly D, Bradshaw J, Burruss R, Holloway S, Christensen NP, et al. CO_2 storage capacity estimation: methodology and gaps. Int J Greenhouse Gas Control 2007;1(4):430–43. https://doi.org/10.1016/S1750-5836(07)00086-2.
[13] Baghishov I, Abeykoon GA, Wang M, Oyenowo OP, Argüelles-Vivas FJ, Okuno R. A mechanistic comparison of formate, acetate, and glycine as wettability modifiers for carbonate and shale formations. Colloids Surf A Physicochem Eng Asp 2022; 652:129849. https://doi.org/10.1016/j.colsurfa.2022.129849.
[14] Bai M, Sun J, Song K, Li L, Qiao Z. Well completion and integrity evaluation for CO_2 injection wells. Renew Sustain Energy Rev 2015;45:556–64. https://doi.org/10.1016/j.rser.2015.02.022.
[15] Bajaj JS. Carbon credit and climate change Nexus. In: Bandh SA, editor. Climate change. Cham: Springer; 2022. https://doi.org/10.1007/978-3-030-86290-9_14.
[16] Benson SM, Cole DR. CO_2 sequestration in deep sedimentary formations. Elements 2008;4(5):325–31. https://doi.org/10.2113/gselements.4.5.325.
[17] Bentham M, Kirby M. CO_2 storage in saline aquifers. Oil Gas Sci Technol 2005;60 (3):559–67. https://doi.org/10.2516/ogst:2005038.
[18] BloombergNEF. Carbon Offset Prices Could Increase Fifty-Fold by 2050. BloombergNEF; January 10, 2022. Retrieved from, https://about.bnef.com/blog/carbon-offset-prices-could-increase-fifty-fold-by-2050/.
[19] Bruant R, Guswa A, Celia M, Peters C. Safe storage of CO_2 in deep saline aquifers. Environ Sci Technol Washington DC 2002;36(11):240A–5A.
[20] Budinis S, Krevor S, Dowell NM, Brandon N, Hawkes A. An assessment of CCS costs, barriers, and potential. Energ Strat Rev 2018;22:61–81. https://doi.org/10.1016/j.esr.2018.08.003.
[21] Bungert D, Maikranz S, Sundermann R, Downs J, Benton W, Dick MA. The evolution and application of formate brines in high-temperature/high-pressure operations. In: IADC/SPE drilling conference. OnePetro; 2000, February. https://doi.org/10.2118/59191-MS.
[22] Chen Y, Vise A, Klein WE, Cetinbas FC, Myers DJ, Smith WA, et al. A robust, scalable platform for the electrochemical conversion of CO_2 to formate: identifying pathways to higher energy efficiencies. ACS Energy Let 2020;5(6):1825–33. https://doi.org/10.1021/acsenergylett.0c00860.
[23] Christie MA, Blunt MJ. Tenth SPE comparative solution project: a comparison of upscaling techniques. SPE Reserv Eval Eng 2001;4(4):308–17. https://doi.org/10.2118/72469-PA.
[24] Computer Modelling Group. STARS Version 2018 User's Guide. Calgary, Alberta, Canada: Computer Modelling Group; 2018.
[25] Congressional Research Service. Federation of American Scientists. Retrieved December 28, 2021, from, https://sgp.fas.org/crs/misc/IF11455.pdf; 2021, June 8.
[26] Crolet JL. Acid corrosion in wells (CO_2, H_2S): metallurgical aspects. J Petrol Tech 1983;35(08):1553–8. https://doi.org/10.2118/10045-PA.
[27] Downs JD. High-temperature stabilisation of xanthan in drilling fluids by the use of formate salts. Phys Chem Coll Interf Oil Prod 1992;50:197–202.
[28] Downs JD. A review of the impact of the use of formate brines on the economics of deep gas field development projects. In: SPE Deep Gas Conference and Exhibition OnePetro; 2010, January. https://doi.org/10.2118/130376-MS.
[29] Downs JD. Formate Brines: Novel Drilling and Completion Fluids for Demanding Environments. SPE International Symposium on Oilfield Chemistry, New Orleans, Louisiana, March 1993. 1993. https://doi.org/10.2118/25177-MS.
[30] Ebigbo A, Class H, Helmig R. CO_2 leakage through an abandoned well: problem-oriented benchmarks. Comput Geosci 2007;11:103–15. https://doi.org/10.1007/s10596-006-9033-7.
[31] European Commission CORDIS. Oxalic acid from CO_2 using electrochemistry at demonstratioN scale. 2022, May 26. https://doi.org/10.3030/767798.
[32] Fanchi JR. Rock–fluid interactions. In: Fanchi JR, editor. Integrated reservoir asset management. Gulf Professional Publishing; 2010. p. 167–85. https://doi.org/10.1016/B978-0-12-382088-4.00010-4.
[33] Farvardini M. The sedimentological distribution of upper brent, Oseberg field, North Sea (Dissertation). Retrieved from, http://urn.kb.se/resolve?urn=urn:nbn:se:uu:diva-312874; 2017.
[34] Fitts JP, Peters CA. Caprock fracture dissolution and CO_2 leakage. Rev Mineral Geochem 2013;77(1):459–79. https://doi.org/10.2138/rmg.2013.77.13.
[35] Global CCS Institute. Unlocking private finance to support CCS investments. Retrieved from, https://www.sustainablefinance.hsbc.com/mobilising-finance/-/media/gbm/reports/sustainable-financing/carbon-capture-storage-ccs.pdf; 2021.
[36] Godec M. Acquisition and development of selected cost data for saline storage and enhanced oil recovery (EOR). United States. 2014. https://doi.org/10.2172/1557133.
[37] Gozalpour F, Ren SR, Tohidi B. CO_2 EOR and storage in oil reservoir. Oil Gas Sci Technol 2005;60(3):537–46. https://doi.org/10.2516/ogst:2005036.
[38] Grigioni I, Sagar LK, Li YC, Lee G, Yan Y, Bertens K, et al. CO_2 electroreduction to formate at a partial current density of 930 mA cm–2 with InP colloidal quantum dot derived catalysts. ACS Energy Lett 2020;6(1):79–84.
[39] Gupta N, Sass B, Chattopadhyay S, Sminchak J, Wang P, Espie T. Geologic storage of CO_2 from refining and chemical facilities in the midwestern US. Energy 2004;29 (9–10):1599–609. https://doi.org/10.1016/j.energy.2004.03.062.
[40] Hassanzadeh H, Pooladi-Darvish M, Keith DW. Accelerating CO_2 dissolution in saline aquifers for geological storage - mechanistic and sensitivity studies. Energy Fuel 2009;23(6):3328–36. https://doi.org/10.1021/ef900125m.
[41] Hietala J, Vuori A, Johnsson P, Pollari I, Reutemann W, Kieczka H. Formic acid. In Ullmann's encyclopedia of industrial chemistry, (Ed.). 2016. https://doi.org/10.1002/14356007.a12_013.pub3.
[42] Hosa A, Esentia M, Stewart J, Haszeldine S. Injection of CO_2 into saline formations: benchmarking worldwide projects. Chem Eng Res Design 2011;89(9):1855–64. https://doi.org/10.1016/j.cherd.2011.04.003.
[43] Howard SK. Formate brines for drilling and completion: state of the art. In: SPE Annual Technical Conference and Exhibition, Dallas, Texas, October 1995; 1995. https://doi.org/10.2118/30498-MS.
[44] Howard S, Chrenowski M. Corrosion in formate brines - 20 years of laboratory testing and field experience. In: In Offshore Technology Conference-Asia OnePetro; 2014, March. https://doi.org/10.4043/24983-MS.
[45] IEA (2019). Putting CO2 to Use, IEA, Paris https://www.iea.org/reports/putting-co2-to-use.
[46] Irlam L. Global costs of carbon capture and storage16. Global CCS institute; 2017.
[47] Jarvis SM, Samsatli S. Technologies and infrastructures underpinning future CO_2 value chains: A comprehensive review and comparative analysis. Renew Sustain Energy Rev 2018;85:46–68. https://doi.org/10.1016/j.rser.2018.01.007.
[48] Jouny M, Luc W, Jiao F. General techno-economic analysis of CO_2 electrolysis systems. Indust Eng Chem Res 2018;57(6):2165–77. https://doi.org/10.1021/acs.iecr.7b03514.
[49] Kim M, Kim C, Lee H, Kim K. Temperature dependence of dissociation constants for formic acid and 2,6-dinitrophenol in aqueous solutions up to 175 °C. J Chem Soc Faraday Trans 1996;92(24):4951–6. https://doi.org/10.1039/FT9969204951.
[50] Kumar A. Characterization of reservoir Fluids based on perturbation from n-alkanes. [doctoral dissertation, University of Alberta]. Education and research archive. 2016. https://doi.org/10.7939/R3PR7N024.
[51] Kumar S, Foroozesh J, Edlmann K, Rezk MG, Lim CY. A comprehensive review of value-added CO_2 sequestration in subsurface saline aquifers. J Nat Gas Sci Eng 2020;81:103437. https://doi.org/10.1016/j.jngse.2020.103437.
[52] Law DHS, Bachu S. Hydrogeological and numerical analysis of CO_2 disposal in deep aquifers in the Alberta sedimentary basin. Energ Conver Manage 1996;37(6–8): 1167–74. https://doi.org/10.1016/0196-8904(95)00315-0.
[53] Lee MY, Park KT, Lee W, Lim H, Kwon Y, Kang S. Current achievements and the future direction of electrochemical CO_2 reduction: A short review. Crit Rev Environ Sci Technol 2020;50(8):769–815. https://doi.org/10.1080/10643389.2019.1631991.
[54] Li B, Tchelepi HA, Benson SM. Influence of capillary-pressure models on CO_2 solubility trapping. Adv Water Resour 2013;62:488–98. https://doi.org/10.1016/j.advwatres.2013.08.005.
[55] Li M, Idros MN, Wu Y, Garg S, Gao S, Lin R, et al. Unveiling the effects of dimensionality of tin oxide-derived catalysts on CO_2 reduction by using gas-

diffusion electrodes. React Chem Eng 2021;6(2):345–52. https://doi.org/10.1039/d0re00396d.
[56] Lide DR. CRC handbook of chemistry and physics. 8th ed. CRC Press; 2004. https://doi.org/10.1021/ja0336372.
[57] Nelms RL, Burke RB. Evaluation of oil reservoir characteristics to assess North Dakota carbon dioxide miscible flooding potential. In: Presented at the 12th Williston Basin Horizontal Well and Petroleum Conference, May 2–4, 2004, Minot, North Dakota; 2004, May.
[58] Newell DL, Carey JW, Backhaus SN, Lichtner P. Experimental study of gravitational mixing of supercritical CO_2. Int J Greenhouse Gas Control 2018;71:62–73. https://doi.org/10.1016/j.ijggc.2018.02.013.
[59] Ofei TN, Al Bendary RM, Habte AD. Rheological performance of potassium formate water-based muds for high-temperature wells. In: Awang M, Negash B, Md Akhir N, Lubis L, Md. Rafek A., editors. ICIPEG 2016. Singapore: Springer; 2017. https://doi.org/10.1007/978-981-10-3650-7_63.
[60] Okuno, R. (2022) Novel Fluids for Enhanced Carbon Storage, the 2022 Energi Simulation Summit, September 20 – 21, 2022, Calgary, Alberta, Canada. https://www.youtube.com/channel/UC3HWdYub1tgbnUDTfSsvDTA/videos.
[61] Philips M, Gruter G, Koper M, Schouten K. Optimizing the electrochemical reduction of CO_2 to formate: A state-of-the-art analysis. ACS Sustain Chem Eng 2020;8(41):15430–44. https://doi.org/10.1021/acssuschemeng.0c05215.
[62] Ravagnani AG, Ligero EL, Suslick SB. CO_2 sequestration through enhanced oil recovery in a mature oil field. J Petrol Sci Eng 2009;65(3–4):129–38. https://doi.org/10.1016/j.petrol.2008.12.015.
[63] Ren B, Zhang L, Huang H, Ren S, Chen G, Zhang H. Performance evaluation and mechanisms study of near-miscible CO_2 flooding in a tight oil reservoir of Jilin Oilfield China. J Nat Gas Sci Eng 2015;27:1796–805. https://doi.org/10.1016/j.jngse.2015.11.005.
[64] Ringrose PS, Mathieson AS, Wright IW, Selama F, Hansen O, Bissell R, et al. The in Salah CO_2 storage project: lessons learned and knowledge transfer. Energy Procedia 2013;37:6226–36. https://doi.org/10.1016/j.egypro.2013.06.551.
[65] Rubin ES. CO_2 capture and transport. Elements 2008;4(5):311–7. https://doi.org/10.2113/gselements.4.5.311.
[66] Rumayor M, Dominguez-Ramos A, Perez P, Irabien A. A techno-economic evaluation approach to the electrochemical reduction of CO_2 for formic acid manufacture. J CO2 Utiliz 2019;34:490–9. https://doi.org/10.1016/j.jcou.2019.07.024.
[67] Sánchez OG, Birdja YY, Bulut M, Vaes J, Breugelmans T, Pant D. Recent advances in industrial CO_2 electroreduction. Curr Opin Green Sustain Chem 2019;16:47–56. https://doi.org/10.1016/j.cogsc.2019.01.005.
[68] Scherer GW, Celia MA, Prevost JH, Bachu S, Bruant R, Duguid A, et al. Leakage of CO_2 through abandoned wells: Role of corrosion of cement. In: Carbon dioxide capture for storage in deep geologic formations. vol. 2. Amsterdam, The Netherlands: Elsevier; 2015. p. 827–48.
[69] Shaffer G. Long-term effectiveness and consequences of carbon dioxide sequestration. Nat Geosci 2010;3:464–7. https://doi.org/10.1038/ngeo896.
[70] Sheng, K., Okuno, R., Imran, M., Nakutnyy, P. & Nakagawa, K. (April, 2021). An Experimental Study of Steam-solvent Coinjection for Bitumen Recovery Using a Large-scale Physical Model. In IOR 2021 (Vol. 2021, No. 1, pp. 1-37). European Association of Geoscientists & Engineers. https://www.earthdoc.org/content/papers/10.3997/2214-4609.202133152.
[71] Sinomine Specialty Fluids. Section A2: Brine density and PVT data. In: In Formate Technical Manual; 2019, August. https://formatebrines.com/wp-content/uploads/2019/10/FORMATEMANUAL-A2-Density-and-PVT-Data.pdf.
[72] Sinomine Specialty Fluids. Section A4: viscosity of formate brines. In: In Formate technical manual; 2019, August. https://formatebrines.com/wp-content/uploads/2019/10/FORMATEMANUAL-A4-Viscosity-of-Formate-Brines.pdf.
[73] Somoza-Tornos A, Guerra OJ, Crow AM, Smith WA, Hodge BM. Process modeling, techno-economic assessment, and life cycle assessment of the electrochemical reduction of CO_2: a review. Iscience 2021;24(7). https://doi.org/10.1016/j.isci.2021.102813.
[74] Vilarrasa V, Bolster D, Dentz M, Olivella S, Carrera J. Effects of CO_2 compressibility on CO_2 storage in deep saline aquifers. Transp Porous Media 2010;85(2):619–39. https://doi.org/10.1007/s11242-010-9582-z.
[75] Wang Q, Wu W, Li Q, Zhang D, Yu Y, Cao B, et al. Under-deposit corrosion of tubing served for injection and production wells of CO_2 flooding. Eng Fail Anal 2021;127:105540. https://doi.org/10.1016/j.engfailanal.2021.105540.
[76] Watson F. Analysts see EU carbon prices at Eur56-Eur89/mt by 2030. S&P Global; December 3, 2020. Retrieved from, https://www.spglobal.com/commodityinsights/en/market-insights/latest-news/coal/120320-analysts-see-eu-carbon-prices-at-eur56-eur89mt-by-2030.
[77] Wei N, Li X, Dahowski RT, Davidson CL, Liu S, Zha Y. Economic evaluation on CO_2-EOR of onshore oil fields in China. Int J Greenhouse Gas Control 2015;37:170–81. https://doi.org/10.1016/j.ijggc.2015.01.014.
[78] Wilberforce T, Olabi AG, Sayed ET, Elsaid K, Abdelkareem MA. Progress in carbon capture technologies. Sci Total Environ 2021;761:143203. https://doi.org/10.1016/j.scitotenv.2020.143203.
[79] Williams N. Canada unveils greenhouse gas reduction credits to boost carbon trading market. Reuters. Retrieved from, https://www.reuters.com/business/environment/canada-unveils-greenhouse-gas-reduction-credits-boost-carbon-trading-market-2021-03-05/; March 5, 2021.
[80] Wilson EJ, Johnson TL, Keith DW. Regulating the ultimate sink: managing the risks of geologic CO_2 storage. Environ Sci Technol 2003;37(16):3476–83. https://doi.org/10.1021/es021038+.
[81] Zhang Y, Lashgari HR, Sepehrnoori K, Di Y. Effect of capillary pressure and salinity on CO_2 solubility in brine aquifers. Int J Greenhouse Gas Control 2017;57:26–33. https://doi.org/10.1016/j.ijggc.2016.12.012.
[82] Zhou D, Fayers FJ, Orr FM. Scaling of multiphase flow in simple heterogeneous porous media. In: Paper presented at the SPE/DOE improved oil recovery symposium, Tulsa, Oklahoma, April 1994; 1994. https://doi.org/10.2118/27833-MS.